Energy & Environmental Science

REVIEW

View Article Online
View Journal | View Issue

Cite this: *Energy Environ. Sci.*, 2015, **8**, 3109

Application of computational chemistry in understanding the mechanisms of mercury removal technologies: a review

Lixia Ling,[ab] Maohong Fan,*[a] Baojun Wang*[c] and Riguang Zhang[c]

Received 21st July 2015,
Accepted 28th July 2015

DOI: 10.1039/c5ee02255j

www.rsc.org/ees

The control of mercury in flue gas is challenging, and many investigators have focused on different mercury removal technologies. The application of computational chemistry in understanding mercury removal mechanisms will help to modify and design mercury removal materials, thereby improving the efficiency of the removal of mercury in flue gas. Therefore, a review of theoretical studies on the adsorption and oxidation of mercury has been undertaken in the current study. In this contribution, the homogeneous oxidation mechanisms of Hg^0 as well as heterogeneous interactions including adsorption of mercury species and oxidation of Hg^0 on activated carbon, metals, metal oxides and other materials have been summarized. In addition, possible future directions of theoretical calculations on understanding the removal of mercury are outlined.

1. Introduction

The demand for energy has been growing rapidly in recent years with continuing economic development and improvement in worldwide living standards. Coal has remained one of the main sources of primary energy for decades due to its low cost and broad availability among the different fossil fuels, and it plays a strategic role in medium-to-long-term energy production systems.[1,2] On the other hand, utilization of coal produces more pollutants, such as SO_2 and NO_x, than other fossil fuels, and more greenhouse gases, CO_2, and toxins, such as mercury.[3–5] In particular, mercury is a leading concern because of its volatility, persistence, and neurological health impacts.[6–8] In December 2011, the United States Environmental Protection Agency (U.S. EPA) issued the first national standards – Mercury and Air Toxics Standards (MATS). The aim is to limit the release of mercury, acid gases, and other toxic species from coal-fired power plants.[9]

The mercury in coal-derived flue gas is mainly present as elemental mercury (Hg^0), oxidized mercury (Hg^{2+}), and particulate mercury (Hg^p).[10,11] The outer electronic configuration of Hg^0 is $5d^{10}6s^2$,[119] and all orbitals are filled with electrons and there is no unoccupied orbital. Therefore, Hg^0 is the most difficult species to be removed from flue gas due to its exceedingly high volatility, low water solubility, and relative chemical inertness.[12–15] Due to its water-solubility, Hg^{2+} can easily enter water and be converted to methyl mercury (MeHg), and then enter the food chain by bioaccumulation, thereby leading to birth defects or influencing human health.[16,17] Hg^p has a relatively short atmospheric lifetime and spreads by airborne processes,[18] which may cause respiratory and chromosome damage.[14,19] Many sorbents have been used to remove mercury from flue gas, and adsorption and oxidization processes have also been detected. Homogeneous mercury oxidation, mercury adsorption on different materials, and heterogeneous mercury oxidation have been summarized by Wilcox *et al.*[20] Dranga *et al.*[21] focused on laboratory and plant scale investigations of noble metal and transition metal oxide based catalysts and novel methods in the area of catalytic mercury oxidation. The advantages and disadvantages of different heterogeneous catalytic oxidation catalysts of mercury, and the influence of various acidic gases have also been reviewed during experiments on mercury removal.[22] However, a better understanding of mercury removal mechanisms at the molecular-electronic level will help modify and design mercury removal materials, thereby improving the efficiency of removal in flue gas.

Wilcox at Stanford University,[23–28] Zheng at Huazhong University of Science and Technology,[29–32] and other researchers[33–35] have reported the adsorption and oxidation mechanism of mercury species on different metals, metal oxides, and other material surfaces by using theoretical calculation methods. We have also done some previous work in this field.[36–38] The nature of adsorption and oxidation of mercury has been established. Although some reviews focusing on mercury removal technologies

[a] *Department of Chemical and Petroleum Engineering, University of Wyoming, 1000 E University Ave., Laramie, WY 82071, USA. E-mail: mfan@uwyo.edu*
[b] *Research Institute of Special Chemicals, Taiyuan University of Technology, Taiyuan 030024, Shanxi, People's Republic of China. E-mail: lling@uwyo.edu*
[c] *Key Laboratory of Coal Science and Technology (Taiyuan University of Technology), Ministry of Education and Shanxi Province, Taiyuan 030024, Shanxi, People's Republic of China. E-mail: wangbaojun@tyut.edu.cn*

including the preparation, activity and stability of catalysts have been reported,[20–22] a critical review of the recent advances in the application of theoretical calculation methods for understanding mercury removal mechanisms in flue gas is lacking.

In the present work, the homogeneous oxidation of mercury with different oxidants, such as Cl_2, HCl, ClOH and Br species, will be briefly summarized. Another aspect discussed in this review is the heterogeneous reaction of mercury on different surfaces, which may serve to both adsorb and oxidize Hg. Therefore, the adsorption and heterogeneous oxidation of mercury on activated carbon, metal and metal oxides are reviewed. Finally, analysis and future work will be discussed. These sections will focus on the application of theoretical calculation methods, such as density functional theory (DFT) and *ab initio* methods, for mercury removal, and the corresponding experiments will be compared with these theoretical results. This will shed light on fundamental clues for exploring new materials to remove mercury from flue gas.

2. Homogeneous oxidation of mercury

The homogeneous oxidation of mercury using different oxidants has been studied without any catalysts by using theoretical methods. Some kinetic parameters can be obtained, which are not available or difficult to deduce from experiments. It will help the design of more effective control technologies to prevent their release into the atmosphere.

The DFT method along with Becke' three-parameter hybrid exchange functional and the Lee–Yang–Parr correlation (B3LYP) with the RCEP60VDZ basis set using Gaussion 03 was employed to study the oxidation mechanism of Hg^0 without catalysts, while Cl_2, HCl, Cl, O and HOCl are used as oxidants.[39,40] In DFT, the electron density of the compound or element is calculated rather than the individual electron wave functions. It focuses on the valence electrons since those have a chance for interaction rather than the shielded electrons closer to the core. B3LYP is one of the functionals of DFT, which can produce fairly accurate bond energies and thermodynamic properties of reactions.[41] RCEP60VDZ of the relativistic effective core potentials represents 60 core electrons of the mercury atom, which is derived from numerical Dirac–Fock wave functions using an optimizing process based upon the energy-overlap functional. The program accurately predicts both the bond distances and vibrational frequencies of the elements and compounds in reactions. Rice–Ramsberger–Kassel–Marcus (RRKM) theory was used to predict rate constants, and the rate constants within 298.15–2000 K show that Cl_2 and HOCl play a major role in the oxidation of mercury with HCl, and the atomic chlorine is likely involved in the dominant oxidation pathway because Hg oxidation is primary carried out through a Cl atom recycling process.[42] In addition, the rate constants from 298 to 2000 K decrease as the temperature increases for reactions (R1) and (R2), whereas the insertion reaction (R3) is found to proceed very slowly with large pre-exponential factors. It will provide fundamental information for the removal of mercury.

$$HgCl + Cl \leftrightarrow HgCl_2 \quad (R1)$$

$$Hg + O \leftrightarrow HgO \quad (R2)$$

$$Hg + Cl_2 \leftrightarrow HgCl_2 \quad (R3)$$

In addition, a series of mercury reactions may take place in the flue gases of coal combustion;[43] the reaction enthalpies are listed in Table 1. An *ab initio* method, Quadratic Configuration Interaction with Single and Double Excitations with the RCEP28DVZ basis set (QCISD/RCEP28DVZ), was chosen to study the reaction mechanism according to a comparison of theoretically determined geometries, frequencies, and reaction enthalpies with experimental values. Furthermore, the kinetic parameters over the temperature range of 298–1500 K are shown in Table 2, which have not been obtained from the experiment due to its difficulty. These can be incorporated into the development of kinetic modes for predicting the mercury speciation. In addition, the effect of different gases on the oxidation of Hg by Cl-containing species has been studied. O_2 weakly promotes homogeneous Hg oxidation, whereas moisture is a stronger inhibitor. NO can promote or inhibit homogeneous Hg oxidation depending on its concentration.[42]

Table 1 Reaction enthalpies of mercury reactions (eV)[43]

		Level of theory							
		QCISD		B3PW91		B3LYP			MP2
Reaction	Exp.	RCEP	ECP	RCEP	ECP	RCEP	ECP	LANL	SDD
Hg + HCl = HgCl + H	3.40	3.22	2.91	3.33	2.98	3.43	3.11	3.23	2.36
Hg + HOCl = HgCl + OH	1.35	0.94	0.63	1.26	0.90	1.29	0.97	1.08	0.63
HgCl + HCl = $HgCl_2$ + H	0.89	0.95	0.78	1.12	0.85	1.25	0.98	1.45	0.16
HgCl + Cl_2 = $HgCl_2$ + Cl	−1.07	−1.29	−1.46	−0.81	−1.07	−0.80	−1.07	−0.60	−1.98
Hg + Cl = HgCl	−1.08	−1.15	−1.46	−1.13	−1.48	−1.01	−1.33	−1.21	−0.68
Hg + Cl_2 = HgCl + Cl	1.43	0.98	0.67	1.40	1.05	1.35	1.06	1.20	0.23
Hg + Cl_2 = $HgCl_2$	−2.15	−2.44	−2.91	−1.94	−2.56	−1.81	−2.40	−1.79	−2.66
HgCl + Cl = $HgCl_2$	−3.59	−3.42	−3.59	−3.34	−3.60	−3.19	−3.46	−2.99	−2.89
HgCl + HOCl = $HgCl_2$ + OH	−1.15	−1.33	−1.50	−0.96	−1.22	−0.89	−1.16	−0.69	−1.58
Hg + 2HCl = $HgCl_2$ + H_2	−0.24	−0.30	−0.78	0.03	−0.58	0.14	−0.46	0.13	−1.16
Average absolute error		0.21	0.45	0.16	0.25	0.22	0.20	0.36	0.76

Note: B3PW91 denotes Perdew−Wang 91 for correlation and Becke-three for exchange; RCEP denotes RCEP28DVZ; ECP denotes ECP28MWB; LANL denotes Los Alamos National Laboratory 2 double ζ (LANL2DZ) basis set; MP2 is second order Møller−Plesset perturbation theory.

Table 2 Kinetic parameters (T = 298–1500 K, P = 1 atm)[43]

No.	Reaction	A (cm^3 mol^{-1} s^{-1})	E_a (eV)	Rate expression (cm^3 mol^{-1} s^{-1})
1	Hg + HCl = HgCl + H	1.69×10^{14}	3.86	$k = 1.69\times10^{14}$ $e^{-44\,821/T}$
2	Hg + HOCl = HgCl + OH	1.14×10^{14}	0.64	$k = 1.14 \times 10^{14}$ $e^{-7490/T}$
3	Hg + ClO = HgO + Cl	1.81×10^{12}	2.20	$k = 1.81 \times 10^{12}$ $e^{-25\,465/T}$
4	Hg + Cl_2 + M = $HgCl_2$ + M	1.04×10^{14}	1.71	$k = 1.04 \times 10^{14}$ $e^{-19\,872/T}$
5	Hg + N_2O = HgO + N_2	7.35×10^{14}	1.91	$k = 7.35 \times 10^{14}$ $e^{-22\,110/T}$
6	Hg + O_3 = HgO + O_2	1.44×10^{14}	1.40	$k = 1.44 \times 10^{14}$ $e^{-16\,258/T}$
7	HgO + HCl = HgCl + OH	2.36×10^{13}	3.40	$k = 3.32 \times 10^{13}$ $e^{-39\,451/T}$
8	HgO + HOCl = HgCl + HO_2	1.75×10^{11}	2.48	$k = 2.54 \times 10^{11}$ $e^{-28\,772/T}$
9	Hg + NO = HgO + N	1.32×10^{13}	7.00	$k = 1.32 \times 10^{13}$ $e^{-81\,205/T}$

A series of Hg–Br reactions have been studied by electronic structure calculations using *ab initio* methods.[44] Theoretical activation barriers show that the combination of Hg with Br is surprisingly easy with the least barrier at 298.15 K according to the B3LYP/ECP60MDF, B3LYP/ECP60VDZ and CCSD(T)/AVTZ calculations. This is in agreement with the result obtained by using the RRKM theory together with *ab initio* quantum calculations using the Stevens–Basch–Krauss triple-split CEP-121G basis set.[45] However, further addition of Br to form $HgBr_2$ is slightly easier than the thermal decomposition of HgBr, which is not consistent with the study reported by Goodsite *et al.*[45] They believe that a competition will occur between these two reactions. A similar result is obtained from Hg–Cl reactions; the combination of Cl and Hg with an activation energy of 0.09 eV at the MP2/CEP-121G level[46] is easier than that of dissociation of HgCl with an activation energy of 0.68 eV at the QCISD/60VDZ level,[47] and further addition of Cl to form $HgCl_2$ needs an activation energy of 0.37 eV at B3LYP/60MDF,[40] which is slightly easier than that of dissociation of HgCl. Reaction (R4) has quite high activation barrier, which shows that this reaction is kinetically limited. Upon considering reactions (R5) and (R6), the latter is thermodynamically favored over the former, while the kinetics of the former are favored over that of the latter. This implies that both formation pathways are likely. These reactions, such as (R5) and (R7)–(R9), have low activation barriers.

$$Hg + HBr \rightarrow HgBr + H \quad (R4)$$

$$HgBr + Br_2 \rightarrow HgBr_2 + Br \quad (R5)$$

$$HgBr + HBr \rightarrow HgBr_2 + H \quad (R6)$$

$$HgBr + Br \rightarrow Hg + Br_2 \quad (R7)$$

$$HgBr + H \rightarrow Hg + HBr \quad (R8)$$

$$HgBr_2 + H \rightarrow HgBr + HBr \quad (R9)$$

A detailed review on the homogeneous mercury oxidation kinetics of Hg–Cl and Hg–Br reactions has been reported, in which the consistence of the computational and experimental results was confirmed.[47] Recently, the reaction mechanism of insertion reaction, $Hg + X_2 \rightarrow HgX_2$ (X = Cl, Br and I), has been studied using the B3LYP, ωB97X, B2PLYP, M06, and M06-2X functionals with three different basis sets, LANL2DZ, SDD, and aug-cc-pVTZ-PP. This insertion path is impossible due to its high energy barrier,[48] which agrees with the Br_2 and Cl_2 calculation results of Balabanov *et al.*[49] and Liu *et al.*,[43] respectively. Therefore, the presence of halogen radicals or active surfaces is needed to generate HgX_2 in the modeled experiments, which is in good agreement with the results of previous work.[42] In addition, the halogen radical can be easily formed on the catalyst surface, which indicates that catalysts can considerably lower the energy barriers. Therefore, people have made a lot of efforts in studying heterogeneous oxidation of Hg^0 and great progress has been achieved in this area. However, a review in this area is lacking. Thus, the majority of this review was devoted to fill the gap.

3. Heterogeneous reaction

3.1 Adsorption of mercury on different materials

3.1.1 Activated carbon. Sorbent materials such as activated carbon, metal oxides and pure metals can effectively capture mercury. Among these materials, active carbon is one of the most widely used sorbents because of its high removal capacity.[50] In addition, chlorine-, iodine- and sulfur-promoted activated carbons exhibit a far greater capacity for capturing elemental mercury,[51] and the mercury removal efficiency increases greatly with the increase of oxygen concentration.[52] Physical adsorption is the first step in the removal of mercury for both unpromoted and promoted carbons, while chemical reactions between the adsorbed mercury and sulfur, chlorine, and iodine are the second steps for various promoted activated carbons.[51] Furthermore, other coexistent gases in flue gas have different influences on the removal of Hg using activated carbon.[53] For example, HCl can efficiently improve mercury removal[54] *via* the Deacon reaction, and Cl_2 is formed. Furthermore, O_2 promotes mercury removal, while SO_2 suppresses mercury removal; this is because O_2 is favorable for the Deacon reaction, whereas SO_2 inhibits the Deacon reaction. Hg^0 removal capacity of AC can be improved in the presence of both H_2S and O_2; the possible mechanism is that oxidation of H_2S with O_2 to elemental sulfur, as shown in (R10), may contribute to the Hg^0 removal, and HgS is formed.[55] O_2 is indispensable for Hg^0 removal from the H_2S–SO_2 flue gas system, and the mechanism includes the Clause reaction (R11) and the following reaction (R12).

The reducing gases, CO and H_2 decrease the Hg^0 removal rate, while H_2O promotes Hg^0 removal by activated carbon.[56]

$$H_2S + 1/2O_2 = S_{ad} + H_2O \quad (R10)$$

$$SO_2 + 2H_2S = 3S_{ad} + 2H_2O \quad (R11)$$

$$S_{ad} + Hg = HgS \quad (R12)$$

Halogen embedded activated carbon. Different activated carbon models have been built by fusing several benzenes with different edges, and with halogen groups bonding to these models, with the aim of investigating the effect of halogen on mercury removal by activated carbon.

The mechanism of the adsorption of Hg, HgCl and $HgCl_2$ on activated carbon was studied using the DFT method at B3LYP with the LANL2DZ basis set in the Gaussion 03 package.[57] A single graphene layer with an unsaturated edge on the upper side and chlorine atoms at different sites of the graphene modes was built; this is shown in Fig. 1 and 2. The adsorption energy, E_{ads}, is obtained from the interaction between some molecules and the surface, which can be calculated as

$$E_{ads} = E_{tot}(ads) + E_{tot}(slab) - E_{tot}(ads/slab) \quad (E1)$$

where $E_{tot}(ads)$, $E_{tot}(slab)$ and $E_{tot}(ads/slab)$ are the total energies of the free adsorbate in the gas phase, the bare slab, and the slab with the adsorbate in its equilibrium geometry, respectively.

Hg adsorbs on the unsaturated surface with adsorption energies of 0.62 and 0.64 eV. HgCl is formed when Hg adsorbs on the chloride-containing surface. HgCl and $HgCl_2$ can be adsorbed dissociatively and non-dissociatively; HgCl remains on the surface while stable $HgCl_2$ is not found on the surface. Likewise, HgBr species are more stable on the carbon surface than $HgBr_2$ species according to the plane-wave DFT calculations based on the Perdew–Burke–Ernzerhof functional of the generalized gradient approximation (GGA-PBE) method.[58] Electronic structure calculations have also been carried out to determine the surface reactivity, and DOS calculations indicating that Hg is more stable when it is bound to the edge C atom interacting with a single Br atom bound atop of Hg *via* s- and p-state hybridization of Hg with Br and C p-states.[58] In addition, a different fused-benzene 2 × 2 ring cluster has been built to model activated carbon, and the effect of halogen atoms on Hg adsorption capacity has also been studied using the DFT method at the B3LYP level with the LANL2DZ basis set.[59] Fig. 3 shows the models of mercury adsorbed on activated carbon and halogen-embedded activated carbon, and the adsorption energies and C–X bond distances are listed in Table 3. It can be seen that the adsorption energies of Hg on the halogen-embedded activated carbon are larger than that on the activation carbon, and the order of mercury adsorption is F > Cl > Br > I. Almost an equal promotion effect of Cl and Br on the adsorption of Hg by activated carbon using zigzag models and armchair models was obtained by Liu *et al.*[60] B3PW91 of the DFT method with the RCEP60VDZ basis set uses a relativistic compact effective potential of Stevens *et al.* group[61] in this study. This is in good agreement with experimental results,[62] in which Cl is impregnated into activated carbon, resulting in a significant Hg^0 removal efficiency of 80–90%, compared to original activated carbon, with a Hg^0 removal efficiency of only 10–15%. In addition, bromine-impregnated carbon fiber was prepared to test the removal efficiency of Hg in the presence of NO_x and SO_2.[63] NO or NO_2 promotes the oxidation of Hg^0 to Hg^{2+}, while SO_2 inhibits the adsorption and oxidation of Hg^0 due to SO_2 scavenging the surface bromine species. However, bromine is more effective than chlorine for homogeneous oxidation of mercury through gas-phase reaction.[64]

Oxygen functional group embedded activated carbon. The effect of different oxygen functional groups on the adsorption of Hg on activated carbon has been studied by using the B3LYP functional with the LANL2DZ basis set,[59] and the optimized structures are shown in Fig. 4. Lactone and carbonyl functional groups yield the biggest adsorption energies. Carbonaceous models with zigzag and armchair edges were also built, and

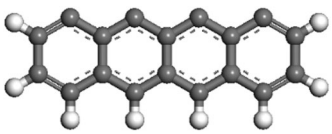

Fig. 1 Optimized geometry of graphene.[57]

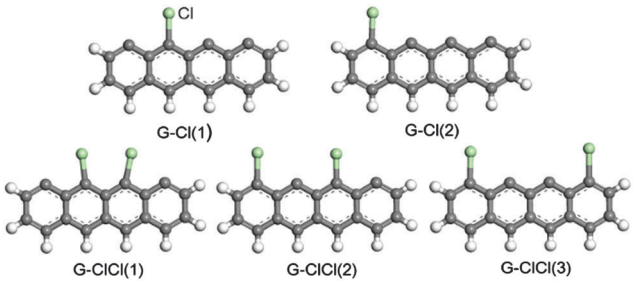

Fig. 2 Graphene modes with chlorine.[57]

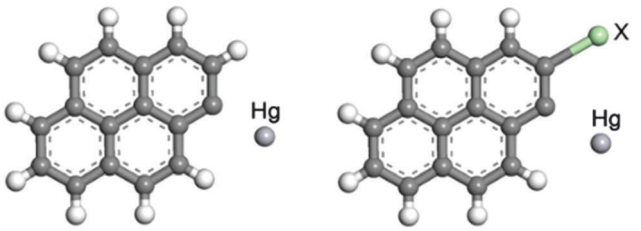

Fig. 3 Cluster models of mercury adsorbed on activated carbon and halogen-embedded activated carbon. X: F, Cl, Br, and I.[59]

Table 3 Adsorption energies and C–X bond distances of Hg associated with the clusters[59]

	Adsorption energies (eV)	C–X bond distances (Å)
AC	−0.19	—
AC-F	−0.42	1.42
AC-Cl	−0.34	1.85
AC-Br	−0.29	1.98
AC-I	−0.23	2.17

the adsorption structures of Hg^0 on the models with different oxygen functional groups are shown in Fig. 5.[60] The DFT method with the B3PW91-RCEP60VDZ basis set was used to calculate adsorption energies, as shown in Table 4. It can be concluded that lactone, carbonyl and semiquinone groups have a promotional effect on Hg^0 adsorption because activities of the neighboring sites of carbonaceous materials with these groups have been increased. In addition, phenol and carboxyl functional groups show physisorption of Hg^0.

Sulfur containing species embedded activated carbon. Elemental sulfur has been impregnated in activated carbon to remove mercury; in this case, temperature does not have a significant effect on Hg^0 adsorption.[65] A chemical reaction mechanism between Hg^0 and S is suggested to explain Hg^0 adsorption when the activated carbon contained sulfur, and HgS is formed. However, HgS can diffuse into the sulfur liquid phase, breaking up sulfur chains to provide additional sulfur terminal atoms to react with mercury.[66] The capture of Hg^0 for activated carbon without sulfur is a physisorption mechanism, due to lower Hg^0 capture at higher temperature. In addition, the effect of different gases in flue gas on the mercury removal capacity has also been investigated.[67]

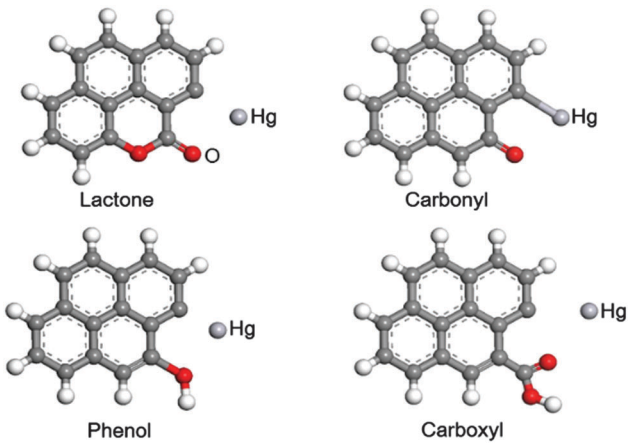

Fig. 4 Activated carbon clusters with oxygen functional groups: lactone, carbonyl, phenol, and carboxyl.[59]

Table 4 C–Hg bond lengths and adsorption energies of Hg^0 adsorption on the carbonaceous surface without and with different oxygen functional groups[60]

Model	C–Hg bond lengths (Å)	E_{ads} (eV)
Zigzag-A	2.29	−0.31
Zigzag-BC	2.32	−0.46
Armchair	2.23	−0.50
Zigzag-carbonyl	2.33	−1.43
Zigzag-carboxyl	2.36	−0.17
Zigzag-lactone	2.27	−1.70
Zigzag-phenol	2.29	−0.45
Zigzag-semiquinone	2.28	−1.31
Armchair-carbonyl	2.32	−1.80
Armchair-carboxyl	2.28	−0.36
Armchair-phenol	2.26	−0.53
Armchair-semiquinone	2.27	−1.24

CO_2, SO_2 and NO had no impact on the adsorption capacity of mercury by sulfur-impregnated activated carbons when the amount of CO_2 is less than 15%, and SO_2 and NO are below 1600 and 500 ppm, respectively; O_2 can increase the uptake capacity to 30%; while moisture decreases the capacity for capturing mercury. Liu *et al.*[68] have studied the effect of SO_2 on mercury adsorption on the carbonaceous surface using the DFT method with the B3PW91-RCEP60VDZ basis set and the cluster model; a six-fused benzene ring model with the unsaturated edge was built to represent the carbonaceous surface. The adsorption structures of Hg on the carbonaceous surface without and with SO_2 are shown in Fig. 6. The adsorption of SO_2 increases the Hg^0 adsorption capacity due to an increase of activity of neighboring sites. However, higher concentrations of SO_2 decrease the adsorption ability because SO_2 competes for the activate sites on the carbonaceous surface with Hg.

Fig. 6 Models for Hg adsorption on the carbonaceous surface without and with SO_2.[68]

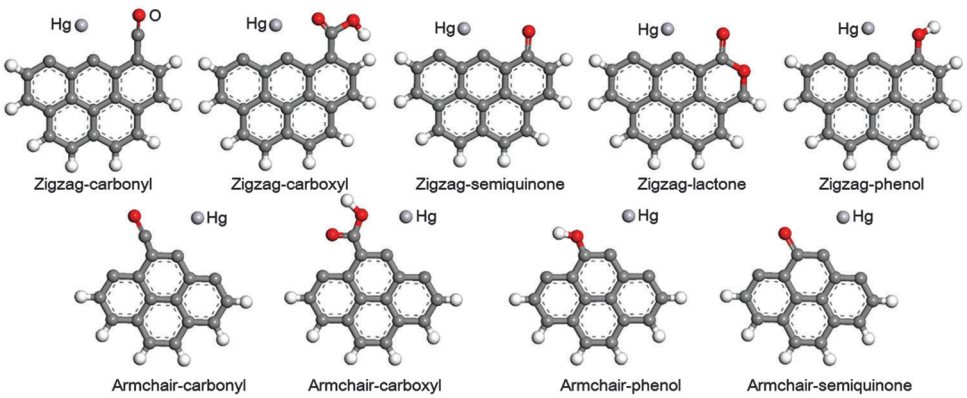

Fig. 5 Adsorption of Hg on the carbonaceous surface with oxygen functional groups: lactone, phenol, carboxyl, carbonyl and semiquinone.[60]

Sulfur containing groups have also been introduced in glass fiber supported activated carbon fibers, and the sulfur atoms were incorporated into the carbon matrix in the form of sulfide and sulfate.[69] The sulfur groups appeared to be more effective for mercury removal than sulfate. The possible mechanism for Hg adsorption by a sulfide group is shown in Fig. 7, which includes three steps: (1) oxidation: Hg^0 is oxidized to Hg^{2+} and forms a double bond with S using two pairs of shared electrons; (2) electron transfer: one electron transfers from the HgS double bond to the C–S single bond, leaving one electron of Hg and one electron of carbon being reactive; and (3) rearrangement: the reactive electron of Hg and the reactive electron of carbon form a single bond.

Activated carbon impregnated with M_xO_y. To improve mercury removal efficiency, impregnation of some metal oxides, such as V_2O_5, MnO_2, Fe_2O_3 and CeO_2, into activated carbon has been studied.

Wang *et al.*[70] prepared the activated coke (AC) supported V_2O_5 (V_2O_5/AC) catalyst. From their work, it can be concluded that the Hg^0 capture capability of V_2O_5/AC was much higher than that of AC. Furthermore, capture increases with an increase in V_2O_5 loading and is promoted by O_2, which indicates an important role of V_2O_5 in Hg^0 oxidation and capture. The removal ability is promoted slightly by SO_2 but is inhibited by H_2O, and increases with an increase in temperature up to 150 °C, when Hg desorption starts. Similarly, AC supported MnO_2, Fe_2O_3[71] and CuO have also been prepared.[72] M_xO_y/AC has higher capability for removing mercury than that of AC, and the trend is MnO_2/AC > Fe_2O_3/AC > CuO/AC. In addition, the Hg^0 removal capability of MnO_2/AC increased with the loading of MnO_2 (1–10 wt%) and temperature (120–200 °C). In the same way, CeO_2 impregnated into activated carbon fiber (ACF) has also significantly enhanced the Hg^0 removal ability of ACF, and the optimized loading value is 6%.[73] The removal ability of Hg^0 increased with an increase in temperature below 150 °C, and then decreased after 150 °C. Both NO and SO_2 have a positive effect on Hg^0 oxidation. At the same time, CeO_2 loaded on AC has been prepared to capture mercury, and the Hg^0 capture capacity of CeO_2/AC is much higher than that of AC.[74] A promoting effect of SO_2 on removing Hg has also been detected, and the Hg^0 capture ability of CeO_2/AC was 50% higher than that of AC when the concentration of SO_2 was 500 ppm, and then decreased slightly when the SO_2 concentration increased to 5000 ppm. HgO and $HgSO_4$ are the main forms of oxidized Hg. In addition, HCl can also result in a higher level of mercury oxidation.

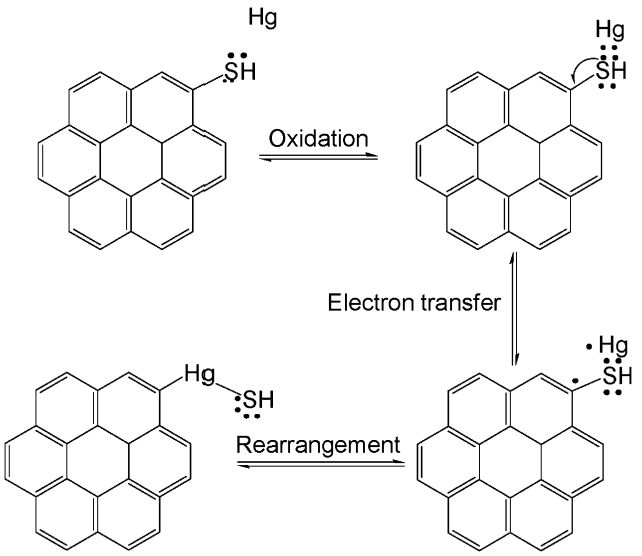

Fig. 7 A possible mechanism for Hg adsorption by a sulfide group.[69]

However, the functions of M_xO_y on different carbon materials are not clear, such as whether M_xO_y increases the activation sites of carbon materials, or carbon materials increases the disparity of M_xO_y, or whether the interaction between M_xO_y and carbon materials is increased or reduced. Furthermore, it has not been established whether an Eley–Rideal (E–R) mechanism, or a Langmuir–Hinshelwood (L–H) mechanism, or a Mars–Maessen (M–M) is the dominant mechanism. Finally, the difference between M_xO_y/AC and M_xO_y has not been determined. These effects need to be explained at molecular-electronic levels by the theoretical calculation method.

3.1.2 Single metal. Copper and some noble metals including gold, silver, platinum and palladium have been used for removing mercury from flue gas, and the interaction mechanisms have been studied by different theoretical methods.

Gold is often the preferred metal for capturing Hg in flue gas due to its high collection efficiency. In addition, it is not influenced by sulfur-containing species, such as SO_2, H_2S, and organic substances.[75] However, the capture efficiency of Hg depends on the temperature.[76] The adsorption of elemental mercury on small neutral, cationic and anionic gold clusters (Au_n, n = 1–6) by using the DFT method has been studied.[77] GGA-PW91PW91 exchange and correlation functionals were selected.[78] For a heavy Au atom, the LANL2DZ basis set and the corresponding Los Alamos relativistic effective core potential (RECP)[79–81] were employed to take scalar relativistic effects into account, including mass velocity and Darwin corrections. The adsorptions of Hg on the three gold clusters are thermodynamically favorable. The adsorption energies of Hg on the cationic Au_n clusters are greater than those on neutral and anionic clusters. Natural bond orbital (NBO) analysis indicates that the flow of electrons in the neutral and charged clusters is mainly due to the s orbitals of Hg and Au. The results of NBO analysis also indicate that the adsorption energy of Hg with Au_n clusters is directly proportional to charge transfer; the greater the charge transfer, the higher the adsorption energy. It can be concluded that frontier molecular orbital theory is a useful tool to predict the selectivity of Hg adsorption.

Lim *et al.*[23] have studied the adsorption of Hg, HgS and HgO on the perfect, vacancy, sulfur and oxygen precovered Au(111) surfaces by using the DFT method with the GGA-PW91 functional. The adsorption strength of Hg on Au(111) increases from −0.42 to −0.55 eV when the number of surface vacancies increases from 0 to 3. However, the adsorption energy decreases with more than three vacancies. Atomic sulfur and

oxygen precovered-Au(111) surfaces lower the Hg stability when Hg adsorbs on the top of S and O atoms. However, a cooperative effect between adjacent Hg atoms is observed as the number of S and Hg atoms increases on the perfect Au(111) surface, resulting in an increase in the magnitude of Hg adsorption. For the adsorption of HgS, the S p-orbitals are strongly hybridized with the Au d-orbitals and shifted to the lower energy level, which is primarily responsible for the interaction of HgS with S bound directly to the Au surface. The d-orbital of Hg interacting with the Au surface is hybridized with the d-orbital of Au between approximately −6 and −3 eV. This contributes to the stability of the HgS molecule on the Au surface; see Fig. 8. Furthermore, the interaction of HgO on the Au(111) surface is similar to the interactions of HgS. The peak corresponding to the HgO interaction is much deeper at approximately −0.72 eV. The Hg d-orbital hybridization of HgO with the Au d-orbital is stronger, more broadened, and more shifted to the lower energy level than that of HgS, which is responsible for the stronger Hg–O interaction than Hg–S on the Au surface.

For the removal of mercury by silver, a small quantity of Ag supported on 4A molecular sieves has been prepared; the study shows that the Ag/4A sieves are active, renewable, and stable for long term operation.[82] In addition, H_2S in natural gas up to 1 ppm will not influence Hg removal under dry operating conditions.

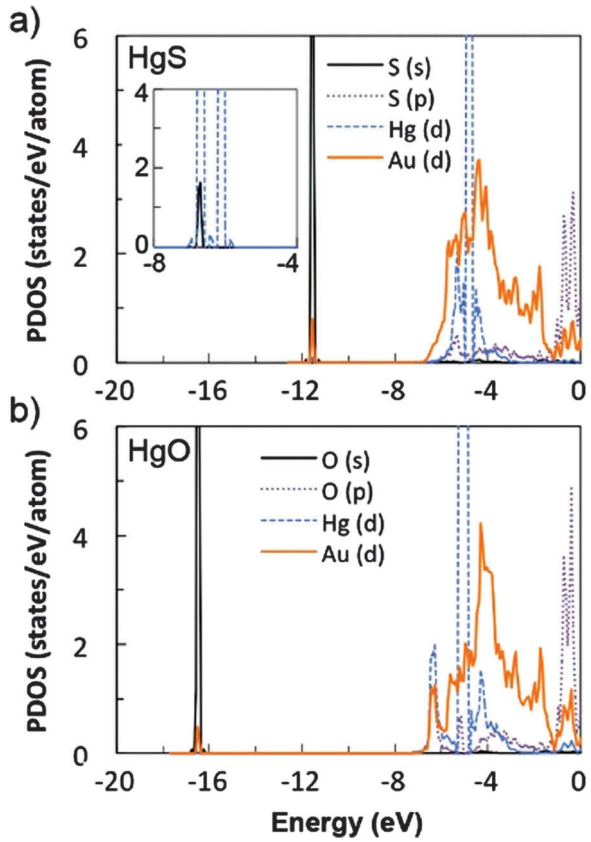

Fig. 8 Projected density of states (PDOS) of (a) HgS and (b) HgO adsorbed on the Au top site of the Au(111)-$p(2 \times 2)$ surface with the Fermi energy referenced at 0 eV. The inset presents the Hg d-orbital and S s-orbital of a gas-phase HgS molecule.[23]

A natural chabazite-based silver nanocomposite (Ag/MC) has also been synthesized to capture mercury from flue gases, and silver nanoparticles are the main active components.[83] A complete capture of mercury by Ag/MC is achieved up to a capture temperature of 250 °C, and the captured mercury can be released by simple heating at 400 °C. In order to understand the removal mechanism, small neutral and charged Ag_n clusters (n = 1–6) have been built, and the adsorption of elemental mercury on these Ag clusters is studied by using the DFT method with the GGA-PBE1PBE functional, in which PBE1PBE/SDD is for Ag and PBE1PBE/ECP60MWB is for Hg.[84] Adsorption energies, Mulliken charge, NBO charge and frontier molecular orbitals are used to provide insights on the interacting mechanism of Hg to different Ag_n clusters. The cluster size and charge affect the adsorption of Hg significantly. On the neutral clusters, the adsorption energies increase first and then decrease. The shorter interaction results in a shorter Hg–Ag bond distance at n = 4, the distance of 2.75 Å between Hg and Ag is the shortest, and the BE of Ag_4Hg is the highest. The adsorption energies for cationic clusters decrease with increasing cluster size, while for the negatively charged Ag_n clusters, the adsorption energies have an odd–even pattern except for Ag_6^-. There is a linear relationship between the lowest unoccupied molecular orbital (LUMO) energies of the neutral and cationic Ag_n clusters and the adsorption energies, and for the anionic Ag_n clusters, there is a linear relationship between the highest occupied molecular orbital (HOMO) energies and the adsorption energies (Fig. 9). NBO analysis shows that neutral and cationic Ag_n clusters are electron acceptors, while anionic clusters are electron donors. The electron flow in the neutral and charged Ag_4Hg is mainly from the s orbital of Ag to the s orbital of Hg. Moreover, for the neutral and anionic Ag_4Hg complex, electron transfer also occurs from the p orbital of Hg to the s orbital of Ag. The more the charge transfer, the higher is the BE.

Dowben *et al.*[85,86] have investigated the adsorption of mercury overlayers on Cu(100) by atom beam scattering, low energy electron diffraction and angle resolved photoemission. It can be concluded that there is an attractive interaction between Hg atoms on the Cu(100) surface. The interactions between Hg with Cu(111) and Cu(001) surfaces have been investigated by using the plane-wave DFT method in the Vienna Ab initio Simulation Package (VASP) code, and projector augmented wave (PAW) potentials were used.[87] The adsorption energies are −0.51 to −0.53 eV and −0.67 to 0.27 eV at different coverages, respectively.

The Hg removal capacity of Pt supported on alumina in a range of different metal loadings from 2 to 9 wt% using Hg vapor in a simulated fuel gas feed has also been investigated.[88] The effect of O_2 and H_2 on the adsorption of Hg has been studied,[89] it shows that O_2 and H_2 do not separately prevent Hg adsorption in the low-temperature region, but when H_2 is passed over a fresh catalyst sample, and then followed by O_2, adsorption of Hg in the low-temperature region is completely blocked. Treating the fresh catalyst, which presumably contains adsorbed O_2, with H_2 does not prevent adsorption of Hg in the

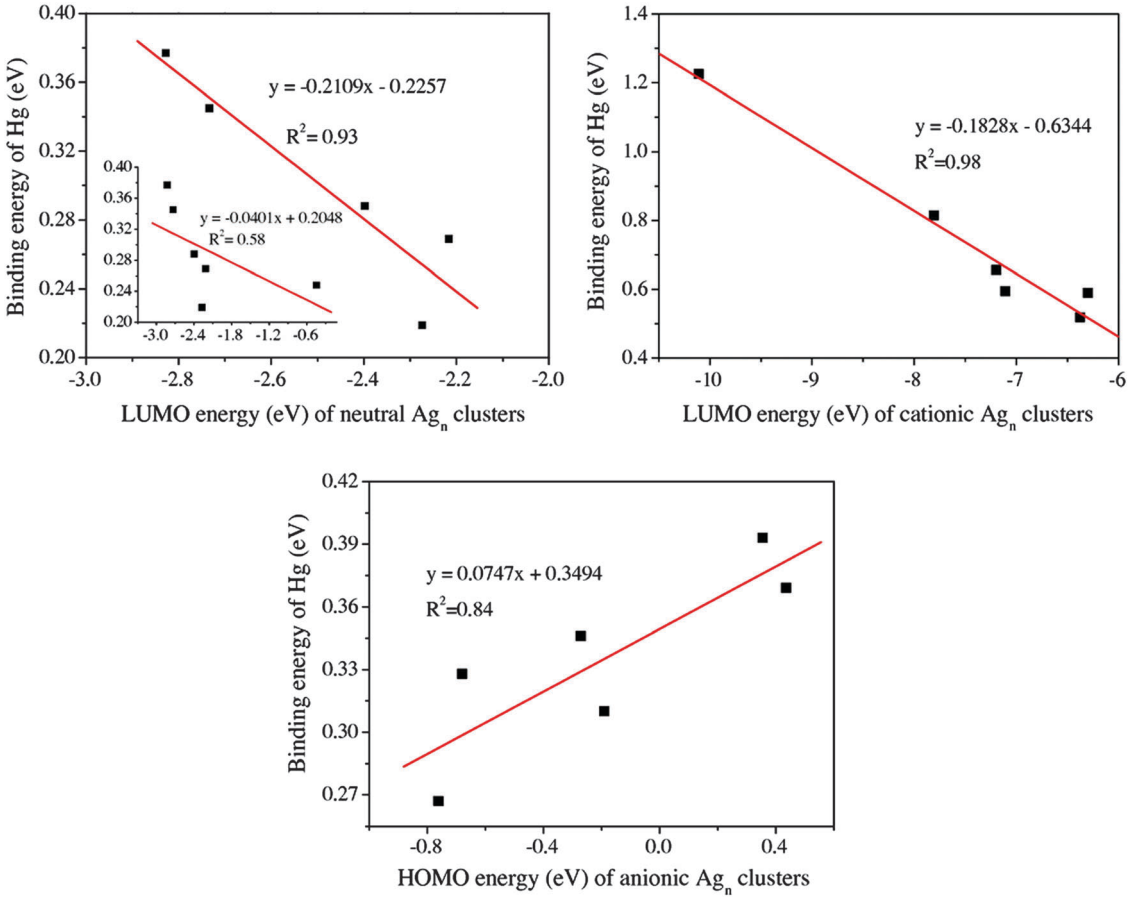

Fig. 9 Relationships between adsorption energies of the most stable complexes and LUMO (HOMO) energies of neutral and charged Ag_n clusters.[84]

low-temperature region. The interactions of Hg with Pt(111) and Pt(001) surfaces at different coverages have been investigated,[87] and the adsorption energy is 0.67–0.75 eV and 0.58–1.09 eV, respectively. The charge density shows that $\Delta Q = -0.18\ e$ for the $p(4 \times 4)$ surface, and the d-band center for the bare Pt surface is located at −2.43 eV. After adsorbing Hg, the d-band is slightly lowered to −2.50 eV.

The enthalpies of amalgamation and oxidation for 22 metals as potential high-temperature Hg sorbents have been calculated by Jain *et al.*;[90] PAW potentials distributed in the VASP package and the GGA-PBE functional were used, and it is found that Pd is the most promising candidate for Hg removal due to its highest amalgamation enthalpy in all metals. This is consistent with the experimental results.[91] Pt and Pd acting as Hg sorbents from fuel gas have been investigated. A solid solution of Hg in Pd was formed when Hg is adsorbed on the Pd/α-Al_2O_3 sorbents, resulting in a substantial increase in the lattice parameter, according to X-ray diffraction (XRD) data, which shows that Pd is significantly better than Pt for removing Hg. Steckel[87] theoretically screened potential metal sorbents for mercury capture using the DFT method, and they also found that Pd is the most effective. Tables 5 and 6 show that the interaction with mercury in the order of increased reactivity over the different metals studied is Ag < Au < Cu < Pt < Pd. The adsorption of Hg_n (n = 1–3) on the perfect, step and

Table 5 Hg adsorption on (111) metal surfaces on hollow sites: θ denotes coverage, E_{ads} denotes adsorption energy, M–Hg and Hg–Hg denote the distance between adsorbed Hg and the substrate or neighboring Hg atoms, respectively[87]

Overlayer	Θ (ML)	E_{ads} (eV)	M–Hg (Å)	Hg–Hg (Å)
$(2\sqrt{3} \times 3)$-Hg/Ag(111)	0.083	−0.34	3.00	8.83
$(2\sqrt{3} \times 3)$-Hg/Au(111)	0.083	−0.36	2.99	8.85
$(2\sqrt{3} \times 3)$-Hg/Cu(111)	0.083	−0.52	2.75	7.70
$(2\sqrt{3} \times 3)$-Hg/Pd(111)	0.083	−0.84	2.81	8.41
$(2\sqrt{3} \times 3)$-Hg/Pt(111)	0.083	−0.75	2.86	8.44
$p(2 \times 2)$-Hg/Ag(111)	0.25	−0.36	3..01	5.88
$p(2 \times 2)$-Hg/Au(111)	0.25	−0.38	3.01	5.90
$p(2 \times 2)$-Hg/Cu(111)	0.25	−0.53	2.78	5.14
$p(2 \times 2)$-Hg/Pd(111)	0.25	−0.81	2.83	5.61
$p(2 \times 2)$-Hg/Pt(111)	0.25	−0.68	2.88	5.62
$(\sqrt{3} \times \sqrt{3}R30°)$-Hg/Ag(111)	0.333	−0.31	3.06	5.08
$(\sqrt{3} \times \sqrt{3}R30°)$-Hg/Au(111)	0.333	−0.32	3.05	5.09
$(\sqrt{3} \times \sqrt{3}R30°)$-Hg/Cu(111)	0.333	−0.48	2.82	4.43
$(\sqrt{3} \times \sqrt{3}R30°)$-Hg/Pd(111)	0.333	−0.80	2.83	4.84
$(\sqrt{3} \times \sqrt{3}R30°)$-Hg/Pt(111)	0.333	−0.67	2.89	4.85
$p(2\times2)$-Hg/Ag(111)	0.5	−0.37	3.09	3.40
$p(2\times2)$-Hg/Au(111)	0.5	−0.35	3.11	3.41
$p(2\times2)$-Hg/Cu(111)	0.5	−0.51	2.87	2.97
$p(2\times2)$-Hg/Pd(111)	0.5	−0.81	2.85	3.24
$p(2\times2)$-Hg/Pt(111)	0.5	−0.69	2.92	3.25

Table 6 Hg adsorption on (001) metal surfaces on hollow sites: θ denotes coverage, E_{ads} denotes adsorption energy, M–Hg and Hg–Hg denote the distance between adsorbed Hg and the substrate or neighboring Hg atoms, respectively[87]

Overlayer	Θ (ML)	E_{ads} (eV)	M–Hg (Å)	Hg–Hg (Å)
$c(4 \times 4)$-Hg/Ag(001)	0.125	−0.50	3.01	8.32
$c(4 \times 4)$-Hg/Au(001)	0.125	−0.61	2.94	8.35
$c(4 \times 4)$-Hg/Cu(001)	0.125	−0.67	2.78	7.26
$c(4 \times 4)$-Hg/Pd(001)	0.125	−1.10	2.83	7.93
$c(4 \times 4)$-Hg/Pt(001)	0.125	−1.09	2.83	7.95
$c(2 \times 2)$-Hg/Ag(001)	0.5	−0.51	3.02	4.16
$c(2 \times 2)$-Hg/Au(001)	0.5	−0.51	3.00	4.17
$c(2 \times 2)$-Hg/Cu(001)	0.5	−0.71	2.80	3.63
$c(2 \times 2)$-Hg/Pd(001)	0.5	−1.08	2.83	3.97
$c(2 \times 2)$-Hg/Pt(001)	0.5	−0.97	2.85	3.98
$c(1 \times 1)$-Hg/Ag(001)	1.0	−0.30	3.30	2.94
$c(1 \times 1)$-Hg/Au(001)	1.0	−0.35	3.39	2.95
$c(1 \times 1)$-Hg/Cu(001)	1.0	0.27	3.14	2.57
$c(1 \times 1)$-Hg/Pd(001)	1.0	−0.67	2.95	2.80
$c(1 \times 1)$-Hg/Pt(001)	1.0	−0.58	3.05	2.81

vacancy-defective Pd(111) (Fig. 10) has been studied.[34] The existence of vacancy and step defects can enhance the mercury adsorption activity of Pd adsorbents (see Table 7). In addition, the γ-Al_2O_3 supported single Pd atom (Fig. 11) shows good Hg adsorption activity as the perfect Pd(111) surface at low Hg coverage, which is well in line with the experiment.[92] The Hg adsorption on Pd/γ-Al_2O_3 weakens the binding of Pd to the γ-Al_2O_3 surface. Moreover, M-substituted (M = Au, Ag, Cu) Pd(111) surfaces also show good Hg adsorption capacity at low Hg coverage (<0.22 eV).[93] These supported and M-substituted catalysts can not only reduce the usage of noble Pd, but also maintain the activity of Pd. A Pd/Al_2O_3 sorbent has also been developed, using an incipient wetness impregnation method, to capture element mercury at high temperature,[94] and it is found that over 90% of the mercury is captured by this sorbent with a Pd loading of 8%. However, the authors suggest that a Pd–Hg amalgam is formed, which is the reason for the capture of Hg.

3.1.3 Alloys. From the above studies, Pd shows excellent Hg removal capacity. However, Pd is an expensive noble metal, thus the cost of Hg removal will be high. Consequently, Pd binary alloys have been studied to predict their removal Hg efficiency. The mechanisms of Hg adsorbing on the binary alloys PdM(111) [M = Au, Ag and Cu] have been investigated. Fig. 12 shows the (111) surface and different adsorption sites.

Table 7 Adsorption energies (eV) for Hg_n (n = 1–3) and the stepwise adsorption energies for the first, second, and third Hg atom on different substrates[34]

Substrates	Hg_1	Hg_2	Hg_3	1st Hg	2nd Hg	3rd Hg
Perfect Pd(111)	−0.84	−1.58	−2.24	−0.84	−0.78	−0.73
Step Pd(111)	−1.52	−2.79	−4.00	−1.52	−1.31	−1.30
Vacancy-defective Pd(111)	−2.25	−3.06	−3.74	−2.25	−0.85	−0.75
Gas phase Pd atom	−0.81	−1.48	−2.02	−0.81	−0.70	−0.61
γ-Al_2O_3(110)	−0.31	−0.44	−0.53	−0.31	−0.16	−0.16
Pd/γ-Al_2O_3(110)	−0.82	−1.21	−1.52	−0.82	−0.43	−0.38

The adsorption energy of Hg shows that Pd is the primary surface atom responsible for improving the interaction of mercury with the surface atoms in both Pd binary alloys and overlays.[25,26] There is a fairly linear relationship between the d-band center of the surface atoms and Hg binding, as shown in Fig. 13. DOS analysis shows that there is a significant overlap between the s- and p-states of Pd and the d-states of Hg, leading to a strong adsorbate–substrate interaction. Recently, the screening method developed by Jain *et al.*[90] has been used to evaluate 17 different binary metal alloys suitable for Hg capture using the VASP package with the PW91 functional.[95] The Gibbs energy of reaction for the Hg adsorption reaction and the competing steam oxidation are calculated by (E2) and (E3), respectively. A negative Gibbs energy of reaction implies that the reaction will move toward the formation of products and is therefore favorable in the case of Hg adsorption and unfavorable in the case of steam oxidation. The $\Delta G_{rxn\text{-}Hg}$ of EuSn, YbSn, BaSn, SmPd, and EuPb is less than 0.21 eV, which shows a favorable Hg adsorption reaction. However, the Gibbs energies of reaction for their respective steam oxidation reactions are roughly an order of magnitude larger, making it very unlikely that these materials would be stable in a syngas environment. Therefore, it can be concluded that none of the materials investigated are suitable for Hg capture at the low concentrations and higher temperatures of the syngas. Those that are predicted to potentially form stable Hg-containing ternary alloys are much more likely to be oxidized by the steam present in the IGCC stream.

$$\Delta G_{rxn\text{-}Hg}(T) = \Delta H^{\circ}_{rxn\text{-}Hg} + T\Delta S^{sub}_{Hg} - RT\ln\left(\frac{p_{Hg}}{p^0}\right) \quad \text{(E2)}$$

$$\Delta G_{rxn\text{-}steam} = \Delta H^{\circ}_{rxn\text{-}steam} - T\Delta S^{\circ}_{rxn\text{-}steam} + RT\ln\left(\frac{p^z_{H_2}}{p^z_{H_2O}}\right) \quad \text{(E3)}$$

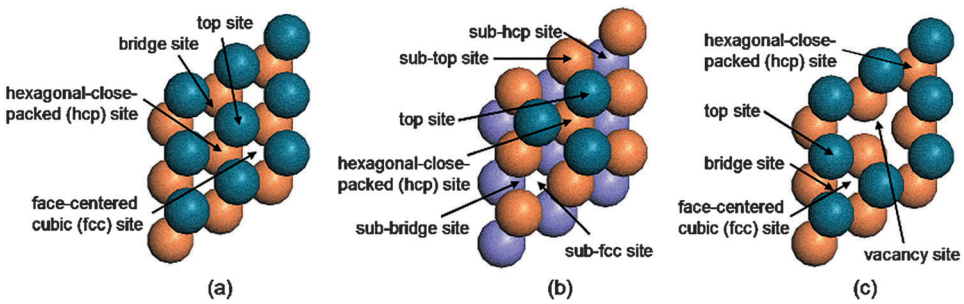

Fig. 10 Top view of the Pd(111) surfaces: the (a) perfect surface, (b) step surface, (c) vacancy-defective surface (first layer In blue, second layer Pd in orange, and third layer Pd atoms in purple).[34]

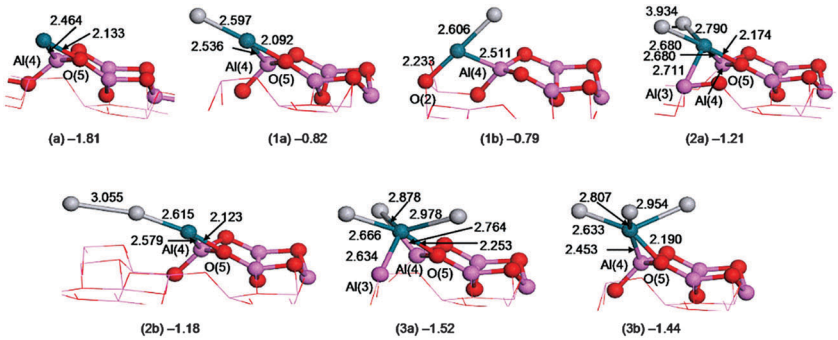

Fig. 11 Optimized adsorption configurations and the adsorption energies (eV) of Hg on Pd/γ-Al_2O_3(110). (Pd, Hg, Al and O atoms are in blue, gray, rose and red, respectively. Bond distances in Å).[34]

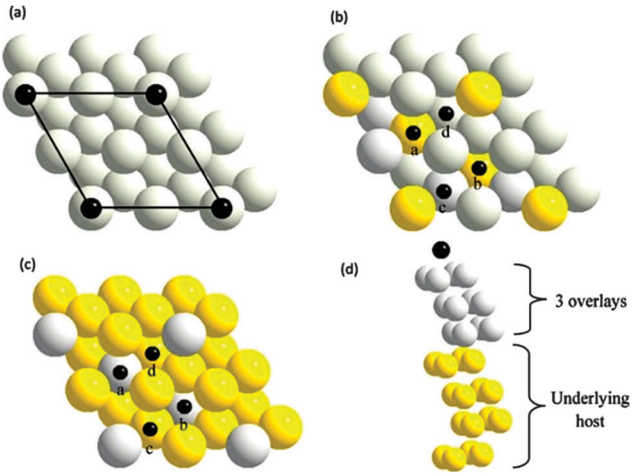

Fig. 12 (a) Scheme of a $p(2 \times 2)$ supercell of (111) surfaces. (b) Threefold adsorption sites of Pd3M binary alloys: a: pure-hcp site, b: pure-fcc site, c: mixed-hcp site, and d: mixed-fcc site. (c) Threefold adsorption sites of PdM3 binary alloys: a: pure-hcp site, b: pure-fcc site, c: mixed-hcp site, and d: mixed-fcc site. (d) Side view of the 3Pd/M(111) structure.[26]

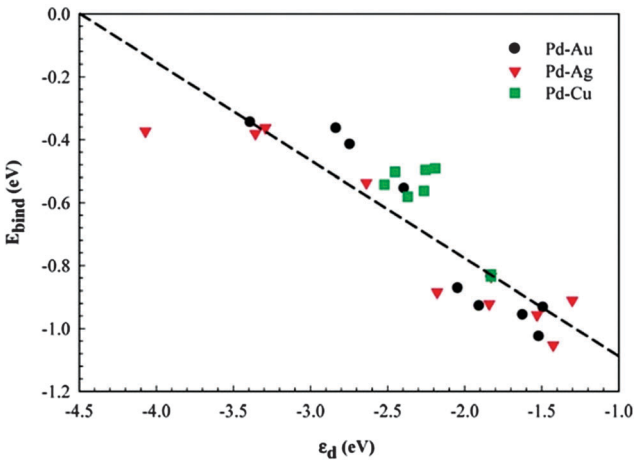

Fig. 13 Center of the d-band of surface atoms of Pd binary alloys and overlayers as a function of Hg binding energy.[26]

3.1.4 Metal oxides. Different synthetic model fly ash components such as Fe_2O_3, CuO and CaO exhibit significant mercury removal ability.[96] In addition, MnO_2-based materials have received a lot of attention because of their high efficiency of mercury removal, better regeneration and high activity over long times.[20]

In order to reveal the ability of Fe_2O_3 for mercury removal, the Fe-terminated nine atomic layer slab models of the α-Fe_2O_3(001) surface with 12 Å vacuum region has been built, as shown in Fig. 14. The mechanisms of mercury and oxidized mercury species such as HgCl and $HgCl_2$ adsorbing on the α-Fe_2O_3(001) surface have been investigated at the level of DFT.[97] All the calculations were performed using the Cambridge Serial Total Energy Package (CASTEP). The GGA with the PBE exchange correlation functional was chosen, a cutoff energy of 300 eV was used in the expansion of the plane wave basis set, and the k point sampling with 0.05 $Å^{-1}$ spacing was utilized. The result shows that Hg^0 is adsorbed on the α-Fe_2O_3(001) surface with the bonding of Fe atoms. Adsorption energy and bond population analysis show that the adsorption of Hg^0 is by physisorption. The oxidized forms of HgCl and $HgCl_2$ can be adsorbed dissociatively or non-dissociatively. HgCl may be favorable for the adsorption of Cl and desorption of Hg, and the dissociation of $HgCl_2$ with the binding of Cl and HgCl on the surface is possibly the dominant interaction pathway. γ-Fe_2O_3 is another form of Fe_2O_3, which can increase the extent of mercury oxidation.[98] However, evidence is insufficient to verify whether γ-Fe_2O_3 reactively captures Hg^0. Perfect and oxygen-deficient γ-Fe_2O_3(001) surfaces have been built (Fig. 15), and adsorption energies of Hg on these surfaces are calculated for different adsorption sites.[99] The GGA-PBE exchange correlation functional was used, and a cutoff energy of 300 eV was employed. Iron cores were described

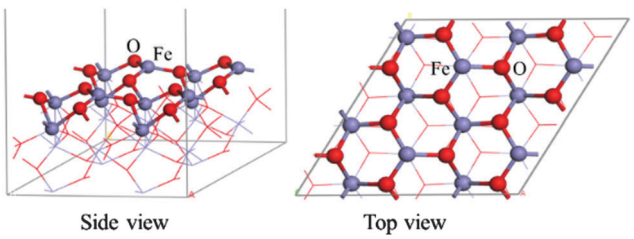

Fig. 14 The slab model and adsorption sites of the α-Fe_2O_3(0001) $p(2 \times 2)$ surface.[97]

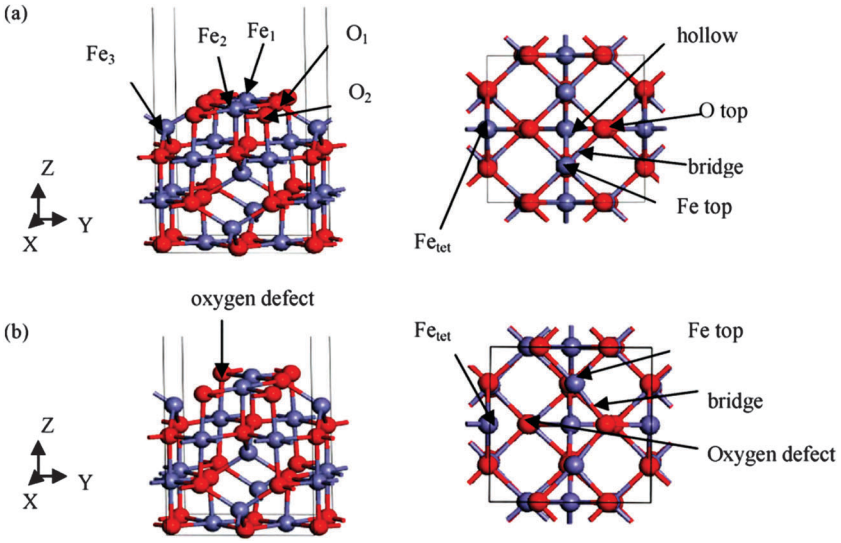

Fig. 15 The computational models. (a) Perfect γ-Fe_2O_3(001) surfaces (side view and top view) and (b) oxygen-deficient γ-Fe_2O_3(001) surfaces (side view and top view) (red spheres represent the O atoms and purple spheres represent the Fe atoms).[99]

by ultrasoft pseudopotentials. It can be obtained that on the perfect γ-Fe_2O_3(001) surface, mercury is preferably adsorbed on the bridge site with an adsorption energy of −0.56 eV. The much stronger interaction occurs at the oxygen vacancy surface with an adsorption energy of −1.40 eV. PDOS analysis shows that there is a formation of the hybridized orbital between Fe and Hg, leading to the strong adsorbate–substrate interaction, which suggests that the presently described processes are all noncatalytic in nature.

However, Fe_2O_3 is a strongly correlated material. The effect of on-site Coulomb interaction between strongly correlated electrons on Fe should be accounted. Standard DFT incorrectly predicts narrow band gaps for bulk hematite and overestimates the interlayer spacing in both hematite bulk and surface structures.[100] DFT+U can locally reduce the one-electron potential for the specified orbitals of the specific atoms (*e.g.*, Fe d orbitals), and thus lower the hybridization with orbitals of the ligands (*e.g.*, O atoms).[101] Accordingly, DFT+U theory should be employed to obtain more accurate results for strong correlated systems.

CaO is one of the primary constituents in novel sorbents that could be used to remove mercury in coal-fired power plants, so the adsorption of mercury and mercury chloride on the CaO(001) surface by means of DFT cluster model calculations has been investigated using the Gaussion 03 package.[102] B3PW91/stevens for the Hg atom and the 6-31* basis set for the Cl atom were used, and the Ca atom was described using the ECP-LANL2 and the LANL2DZ basis set. Different embedding clusters, including shell models, point charge clusters and bare clusters, have been compared. A small adsorption energy of 0.22 eV was found when the elemental mercury molecule is coordinated to the O^{2-} anion, which inferred that mercury was weakly physisorbed at the surface of CaO. $HgCl_2$ adsorption is more complex. When the mercury chloride molecular axis was parallel to the surface, the Hg atom oriented towards the O^{2-} anion and had a large adsorption energy, which meant that mercury chloride adsorbed on the surface is mainly due to chemisorption. In addition, the effect of temperature on adsorption has been studied, and it can be concluded that when the temperature was below 280 °C, the adsorption reaction is spontaneous. However, when the temperature was above 280 °C, the adsorption reaction could not react spontaneously, which implies that high temperature has an adverse effect on adsorption. The surface relaxation has been tested by Blowers *et al.*,[103] and the calculations based on the DFT method were performed using the $Dmol^3$ package[104] in the Accelrys Materials Studio. The DND basis set was employed. LDA with the PWC functional and GGA with the BLYP correlation functional were used to optimize structures and calculate single point energy, respectively. It was found that adsorption energies changed for $HgCl_2$, moving adsorption from being at the borderline of physisorption and chemisorption to being strongly chemisorbed, while Hg and HgCl are unaffected. The minimum cluster size for handling mercury adsorption was 5 × 5 and only two layers of depth were needed. The energetic results show that rumpled CaO surfaces will only weakly physisorb elemental mercury, but could be used to capture $HgCl_2$ from coal combustion flue gases.

Kim *et al.*[105] have also studied the adsorption of Hg, HgCl and $HgCl_2$ on the CaO surface using the cluster model and a periodic structure. The same software and parameters as those reported by Blowers *et al.*'s were used.[103] The adsorption of elemental mercury on the surface is by physisorption with adsorption energies of 0.27–0.32 eV at different model surfaces. The adsorption of HgCl on the CaO(001) surface is predicted through chemisorption, whereas the adsorption energies of $HgCl_2$ on the CaO surface are at the threshold between physisorption and chemisorption. The chlorine atoms released from HCl and Cl_2 in the coal combustion flue gas system greatly enhance the adsorption capability of the CaO according to these predicted results. The effect of temperature on the equilibrium constant for the adsorption of mercury-containing species on the CaO(001) surface was investigated using GGA/BLYP

calculations in the temperature range of 250–600 K. Temperature has a stronger effect on the equilibrium constant for HgCl adsorption than for elemental mercury or $HgCl_2$. The adsorption energy changes for HgCl adsorbed on the surfaces are quite large as the temperature varies because the free radical energy of HgCl is more sensitive to temperature. The equilibrium constant having the steepest changes for HgCl adsorption *versus* temperature is, therefore, intuitive.

Different surfaces have various properties, Hg-containing species adsorbing on another CaO surface have been investigated.[106] One-fold, 2-fold and 3-fold high symmetry adsorption sites of the periodic CaO(100) surface (Fig. 16) have been examined for the species, Hg^0, HgCl, $HgCl_2$ and HgO. VASP software was employed using the GGA-PW91 functional. Hg^0 has a preferred interaction with the surface oxygen atom with an adsorption energy of 0.13 eV, which constitutes a weak interaction. The likely adsorption mechanism of Hg^0 to CaO is physisorption. In comparison to the adsorption of HgCl for both parallel and perpendicular orientations, the adsorption of Cl and desorption of Hg is 0.13 and 0.16 eV more endothermic than these orientations, respectively. This small energy difference indicates that the surface interaction with Cl causes a decrease in the interaction between Cl and Hg, leading to stretching of the HgCl bond and possible desorption of Hg, whereas Cl is strongly bound to O_s sites on the surface. The comparison of adsorption energies of both parallel and perpendicular cases demonstrates that perpendicular adsorption of $HgCl_2$ is not stable on the CaO(100) surface. $HgCl_2$ has a preference to bind at the top-O_s site with an adsorption energy of 0.93 eV. However, HgO may not be stable on the surface, resulting in the desorption of elemental mercury.

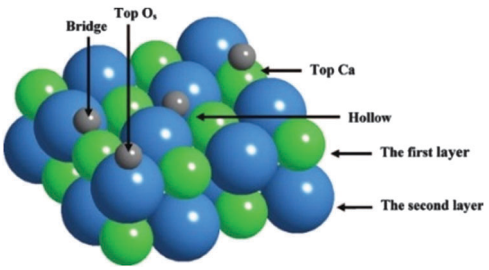

Fig. 16 Illustration of high-symmetry adsorption sites of CaO(100), including the bridge site, hollow site, top Os site and top Ca site.[106]

Manganese oxides (MnO_x) have been considered as potential selective catalytic reduction (SCR) catalysts for Hg removal due to high adsorption ability and high activity in the catalytic oxidation of Hg^0 in flue gas.[107] The Hg^0 removal activity of MnO_x supported on TiO_2 first increases below 400 °C, and then decreases with the increase of calcination temperature.[108] CeO_2 has been added to this sorbent, and MnO_x–CeO_2/TiO_2 shows high activity for Hg^0 oxidation at 150–250 °C under simulated flue gas and SCR flue gas.[109] A 6% Ce–6% MnO_x/Ti-pillared-clay catalyst exhibited good adsorption and oxidation ability in Hg^0 capture, as well as in the absence of HCl.[110] Reactive species on the catalyst surface react adjacently with weakly adsorbed Hg^0 to form Hg^{2+} through the L–H mechanism. NH_3 consumed surface oxygen and limited Hg^0 adsorption, thereby inhibiting Hg^0 oxidation. Gas-phase O_2 can regenerate the lattice oxygen and replenish the chemisorbed oxygen, which facilitates Hg^0 oxidation. 10 ppm HCl plus 4% O_2 resulted in 100% Hg^0 oxidation under the experimental conditions. SO_2 deactivates the capability of the catalyst to oxidize Hg^0 due to its competition with Hg^0 for active sites. NO limits the Hg^0 oxidation due to its occupation of the active sties and consumption of surface oxygen. And H_2O prohibits the Hg^0 oxidation due to competition with HCl and Hg^0 for active adsorption sites.[111] In addition, MnO_x/TiO_2 and MnO_x/CeO_2–TiO_2 materials exhibit high Hg^0 adsorption capacities and excellent NO removal performance both in single-component (NO or Hg^0) tests.[112] Tin(Sn) and iron (Fe) have also been tested for their ability to enhance the MnO_x

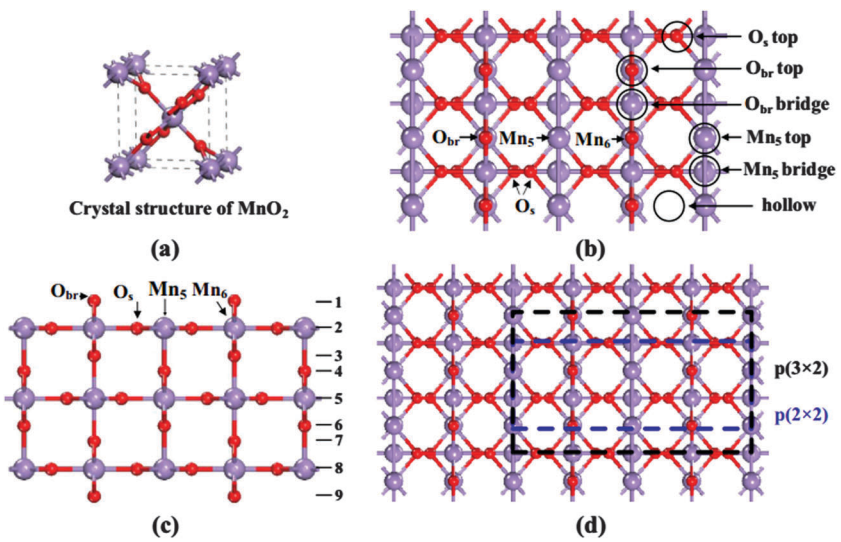

Fig. 17 Slab models of the MnO_2(110) surface. (a) MnO_2 unit cell; (b) top view of MnO_2(110) with six different adsorption sites; (c) side view of MnO_2(110) surface; (d) three different MnO_2(110) surface configurations. The red and purple spheres represent the O and Mn atoms, respectively.[114]

sorbent, and the Fe–Sn–MnO_x complex exhibited excellent performance as a novel mercury sorbent.[113]

In order to explore the removal mechanism of mercury, the periodic slab model of the MnO_2(110) surface has been built, which is shown in Fig. 17, and different mechanisms of Hg-containing species adsorption on this surface have been investigated using the GGA-PBE functional with the DNP basis set in the Dmol^3 package.[114] Hg^0 is strongly adsorbed on the MnO_2(110) surface by chemisorption, and the stable adsorption energies are 0.81 and 0.71 eV at $p(3 \times 2)$ and $p(2 \times 2)$ surface cells, which are different from weak physisorption on the α-Fe_2O_3(001),[97] CaO(001)[105] and CaO(100)[106] surfaces. More electrons are transferred from Hg to surface O than to surface Mn suggesting that Hg^0 is more easily adsorbed on oxygen sites of the MnO_2(110) surface. The adsorption on the MnO_2(110) surface is highly thermally favorable and belongs to chemisorption. HgCl can exist stably on the surface, since the desorption of HgCl is highly endothermic, yet there is still a possibility that HgCl dissociates and Hg desorbs from the surface. $HgCl_2$ can exist stably on the surface because desorption and dissociation are highly endothermic. The temperature effect on equilibrium constants of mercury species has been investigated, which shows that mercury species adsorption on the MnO_2(110) surface is favorable at low temperature and $HgCl_2$ is more easily captured than Hg^0 at higher temperature. However, the oxidation reaction mechanism for Hg^0 over the MnO_x catalyst is not clear, the effect of other components on the removal efficiency of MnO_x is still unclear, and the influence of different gases in flue gas on Hg removal has not been studied at the microscopic level.

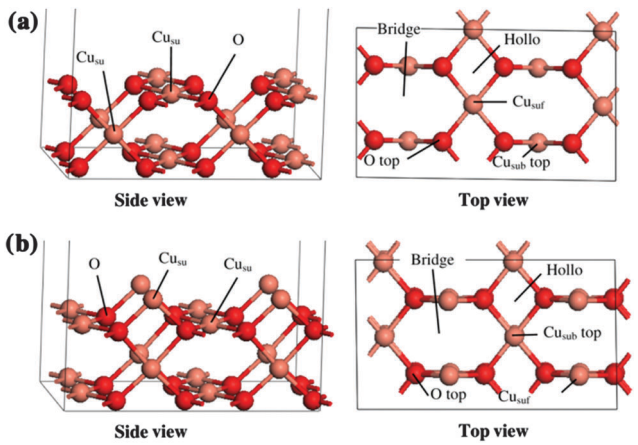

Fig. 18 The top views and side views of CuO(110) surface configurations. (a) O-terminated CuO(110) surface and (b) Cu-terminated CuO(110) surface. The Cu and O atoms are in orange and red, respectively.[32]

Copper based sorbents are widely used to control mercury emission in coal-fired flue gas. The DFT method is a good tool to explore the interaction mechanism. The CuO(110) surface has been chosen to study the binding mechanism of Hg using the first principles quantum mechanical methods.[32] The GGA-PW91 functional was used in the CASTEP package. The O-terminated and Cu-terminated surfaces are both built, see Fig. 18, and Hg which adsorbs on different surface sites is investigated; adsorption energies and bond lengths are shown in Table 8. The results show that Hg binds weakly to the O-terminated CuO(110) surface, which indicates a physisorption mechanism, while Hg is strongly adsorbed on the Cu-terminated CuO(110) surface and chemisorption is the likely adsorption mechanism. The Cu_{sub} top is the most advantageous adsorption site with an adsorption energy of −1.21 eV. The bond population and PDOS are calculated, which also indicate that Hg atoms preferably adsorb on the Cu-terminated CuO(110) surface with the binding of Cu atoms, in which a significant overlap between the d-state of Hg and the s-states of Cu occurs. However, the effect of temperature and flue gas constituents (*e.g.* HCl, NO, SO_2, and NH_3) on the Hg adsorption has not been considered.

3.1.5 Other materials. Some surfactants containing oxygen, nitrogen, and phosphorous show significant mercury removal capacity. A series of uncharged and ionized surfactant models were built,[115] and the adsorption of elemental mercury on these surfactants was calculated by the DFT/B3LYP method. Adsorption energies and Mulliken charge show that the uncharged polar sites have negligible ability to remove mercury from a flue gas stream. Ionized surfactants presented much stronger interactions for mercury and proved the importance of ionization of polar groups for interaction. It is clear that any surfactants containing phosphate or oxygen could be promising in Hg^0 capture. The interaction order of different oxygen-containing ions with mercury is alkyl phosphate > propanoic acid > butanoic acid > decanoic acid > phenoxide > benzoate. This investigation can provide clues and directions for future new removal materials.

3.2 Heterogeneous oxidation of mercury

From the adsorption of mercury containing species on the different metals, metal oxides, and other material surface, we can see that Hg^0 is mainly adsorbed on many surfaces physically or

Table 8 The optimized bond lengths (Å) and adsorption energies (eV) for Hg adsorption on different sites of O-terminated and Cu-terminated CuO(110) surfaces[32]

O-terminated surface				Cu-terminated surface			
Site	R(Hg–O)	R(Hg–Cu)	E_{ads}	Site	R(Hg–O)	R(Hg–Cu)	E_{ads}
O top	3.10	3.68	−0.07	Cu_{sub} top	3.29	2.80	−1.21
Cu_{suf} top	3.06	3.66	−0.11	Cu_{suf} top/bridge		2.61	−1.06
Cu_{sub} top	3.10	4.17	−0.07	Hollow	3.06	2.74	−1.04
Bridge	2.96	3.89	−0.10				
Hollow	3.30	3.38	−0.09				

weakly chemically, and the removal efficiency of mercury will be seriously influenced by temperature and pressure; mercury oxides (HgCl, $HgCl_2$, HgS, and HgO) are mainly chemisorbed on the surfaces. In addition, the mercury oxides can be more easily captured *via* solutions due to their greater solubility, compared with elemental mercury, and HCl, Cl_2 and H_2S can promote Hg^0 capture, because Hg^0 may be oxidized to $HgCl_2$ and HgS.[94] However, mercury in flue gas will be removed efficiently only when Hg^0 can be oxidized to mercury oxides with proper activation energy.

It is well known that Hg oxidation on the different surfaces can occur *via* a L–H[116] or an E–R[117] or a M–M mechanism.[51] In the L–H mechanism, both Hg and Cl_2 (or HCl) are adsorbed on the surface, and subsequently, HgCl or $HgCl_2$ is formed.[14] In contrast, in the E–R mechanism, Cl_2 (or HCl) is adsorbed on the surface, and then a Hg atom from the gas phase directly attacks the adsorbed Cl species leading to the formation of HgCl or $HgCl_2$.[118] The M–M mechanism is the oxidation of Hg^0 by a lattice oxidant to form HgO.[119] Different mechanisms will be processed on the different surfaces. And hence, the oxidation of mercury *via* different materials will be introduced in this section.

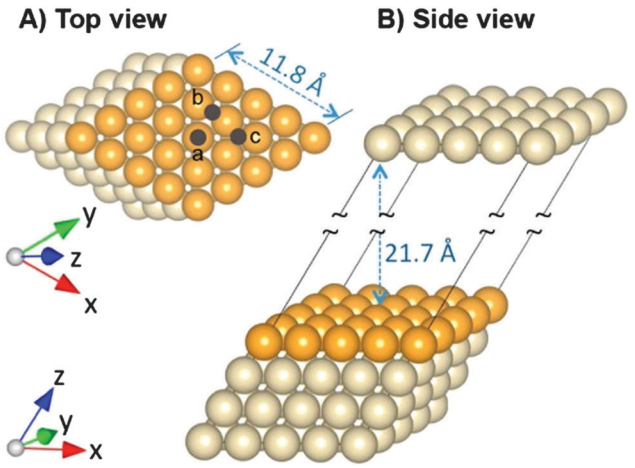

Fig. 19 Perfect Au(111)-$p(4 \times 4)$ surface model: (A) top and (B) side views. Orange and light gray colors represent the top Au surface and the subsurface, respectively. a, b, and c indicate the adsorption sites of atop, bridge, and 3-fold, respectively.[24]

3.2.1 Metal catalysts. For the reaction of Hg^0 with HCl or Cl_2, surface-bound chlorine should be available on the Au surface, based on the fact that Cl_2 can chemisorb to the Au surface.[120] Furthermore, Lim *et al.*[24] studied the mercury oxidation mechanism on the Au(111) surface by using the DFT method with the PW91 functional described by GGA. The perfect Au(111)-$p(4 \times 4)$ surface has been built, as shown in Fig. 19. The L−H mechanism for Hg oxidation was examined, and two Hg oxidation schemes were investigated: *via* the Cl_2 molecule (Cl_2 model) and *via* 2HCl molecules (HCl model). The Climbing Image-Nudged Elastic Band (CI-NEB) method has been employed to calculate the activation energies of HgCl and $HgCl_2$ formation pathways. Fig. 20 shows that the second Cl attachment step is endothermic, and which is the reaction rate-limiting step. It can be concluded that Hg oxidation prefers a pathway in which HgCl and $HgCl_2$ are formed, rather than a pathway directly oxidizing Hg to $HgCl_2$. In the presence of H atoms due to HCl dissociation on the Au surface, the H atoms serve as an "impurity" on the gold surface that consumes the electron charge of the gold atoms, thereby lowering the strength of interaction between the gold atoms and the reaction intermediates, which ultimately enhances the Hg oxidation reaction by lowering the activation energy. However, the experiment showed that HCl had weak oxidizing capability compared with Cl_2, and appreciably inhibited mercury oxidation by Cl_2 using the gold catalyst.[121] Certainly, the HCl molecule interacts with Hg in a bound form on the Au surface in the Hg oxidation mechanism, rather than as gas phase HCl.[122] And another possible reason may be the fact that the surface areas between the experimental conditions and the pure computational

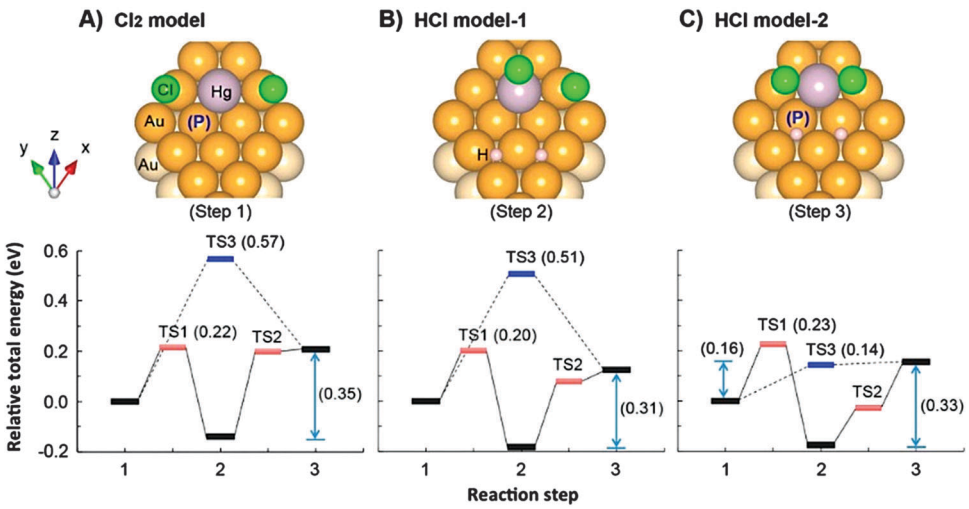

Fig. 20 Reaction pathways of Hg oxidation on perfect Au(111)-$p(4 \times 4)$ surfaces with 9 vacancies *via* the Cl_2 molecule (A) and two HCl molecules (B and C depending on different H atom locations).[24]

environment are different. In addition, the defects reduced the activity of the Au surface, and the oxidation of Hg became more difficult.

The mercury oxidation by HCl on the Pd(100) surface has been studied using the CASTEP plane-wave code with the GGA-PBE functional.[29] Firstly, Hg^0 is strongly adsorbed on the hollow site of the surface with a chemisorption mode; the adsorption energy is 1.01 eV, which is little higher than that on the Pd(111) surface with an energy of 0.84 eV.[34] HCl is chemisorbed on the Pd(100) surface by side-on orientation, and its dissociation occurs with a low energy barrier, and this process is exothermic. Then, adsorbed Hg reacts with HCl that has previously been adsorbed and dissociated on the Pd(100) surface *via* a L–H mechanism; $HgCl_2$ is formed directly without an HgCl intermediate. The result is in good agreement with the experiment, in which Hg^0 can be oxidized to $HgCl_2$ *via* HCl over the Pd/Al_2O_3 catalyst, thereby promoting Hg^0 capture.[94] However, the energy barriers for Hg oxidation on the Pd(100) surface are higher in comparison to that on the Au(111) surface,[24] suggesting that the Hg oxidation reaction occurs more easily by the Au catalyst. In addition, H_2S showed a negative effect on the capture of Hg^0 due to active palladium being occupied by H_2S, and H_2O promoted Hg^0 capture.[94]

3.2.2 Metal oxide catalysts. V_2O_5 is an important SCR catalyst, over which Hg^0 can be oxidized to Hg^{2+}. The effect of HCl, NO, SO_2, SO_3, and NH_3 on Hg^0 oxidization has been investigated. HCl has a strong influence on mercury adsorption as well as mercury oxidation. In the presence of higher concentrations of HCl in the flue gas, elemental mercury is no longer adsorbed but oxidized by the catalyst. With an increase of HCl content from 1 to 50 ppm, Hg oxidation increases from 4% to 63%.[123] However, the rate of oxidation decreases with increasing temperature. The formed $HgCl_2$ is more strongly adsorbed on the catalysts than that of elemental mercury. In addition, the adsorption of both $HgCl_2$ and Hg also decreases with the increase of temperature, even in the absence of HCl.[124] *Ab initio* thermodynamics analysis shows that the adsorption energies of Hg and HgCl decrease with increasing temperature. At high temperature, the entropy loss during adsorption overcomes the adsorption energy, breaking the surface–adsorbate bond. The adsorption of Hg and HgCl is not energetically favored for $T > 300$ K.[27] NO compared to HCl has only a slightly accelerating influence on the Hg oxidization.[124] SO_2 and SO_3 showed a mitigating effect on mercury chlorination to some degree, depending on the concentrations of SO_2 and SO_3, by competing against HCl for SCR adsorption sites.[123] However, Straube *et al.*[124] believe that SO_2 shows a small favorable effect on Hg oxidization. NH_3 shows a small detrimental effect, while the simultaneous presence of NO and NH_3 strongly inhibits the HCl assisted oxidation of elemental mercury. However, the effect of NO, SO_2, SO_3, and NH_3 on Hg oxidization has not been studied by using theoretical methods at the molecular-electronic level.

The effect of halogen species, HF, HCl, HBr, and HI, on the elemental mercury oxidation across the SCR catalyst has been investigated.[125,126] It was shown that HBr and HI both have much stronger effects on mercury conversion than HCl, and the order of impact on Hg^0 oxidation was HBr, HI, and HCl or HF. Addition of HBr at approximately 3 ppm could achieve 80% Hg^0 oxidation. Addition of HI at approximately 5 ppm could achieve 40% Hg^0 oxidation. In comparison to the empty reactor, 40% Hg^0 oxidation could be achieved when HCl addition was up to 300 ppm. However, the enhanced Hg^0 oxidation by addition of HBr and HI seemed not to be correlated to the catalytic effects by both SCR catalysts, which were evaluated.

Different oxidation mechanisms have been provided to illustrate the oxidization of Hg^0 over vanadium-based catalyst. Niksa and Fujiwara[118] suggest that the oxidation of Hg to Hg^{2+} takes place through the E–R mechanism, where HCl competes for surface sites with NH_3 and Hg^0, and contacts these chlorinated sites either from the gas phase or as a weakly adsorbed species. Another mechanism, the Deacon reaction mechanism, has been suggested by Sliger *et al.*[127] It is proposed that Hg oxidation is based on the Cl_2 reaction. Here, Cl_2 is catalytically generated by the interaction of HCl with fly ash and char. Once formed, Cl_2 rapidly reacts with Hg, and the oxidized mercury is partially captured by the char. He *et al.* and Eom *et al.*[14,128] show that the monomeric vanadyl sites on the catalyst surface were found to be responsible for the adsorption of both Hg^0 and HCl, which means that they are active for mercury oxidation. Furthermore, both the Hg and chlorine species undergo heterogeneous reaction with each other. Therefore, the formation of the first layer of Hg with the HCl complex on the surface of the catalyst follows the L–H mechanism. During the oxidization of Hg, the V^{5+} species is transformed to the V^{4+} species, and consumes the lattice oxygen on the surface of the catalyst. It may be *via* the M–M mechanism.[129]

In order to certify which mechanism is favorable for the oxidization of Hg^0 over the V_2O_5 catalyst, a DFT method has been adopted to investigate the interactions of Hg^0, HCl, HgCl and $HgCl_2$ on the $V_2O_5(001)$ surface.[30] LDA-PWC and GGA-BLYP were used to optimize structures and obtain adsorption energies, respectively. The $V_2O_5(001)$ surface was represented by a periodic model, and different adsorption sites were considered, as depicted in Fig. 21. Hg^0 adsorbs on the V_2O_5 surface with an energy of 0.60 eV. The adsorptions of HgCl and $HgCl_2$ on the V_2O_5 surface are mainly by chemisorption. The adsorption energy of HgCl on the V_2O_5 surface is stronger than that of $HgCl_2$, which means that the HgCl-surface is an important intermediate for mercury oxidation. The chlorine species has a strong influence on mercury adsorption as well as mercury oxidation.

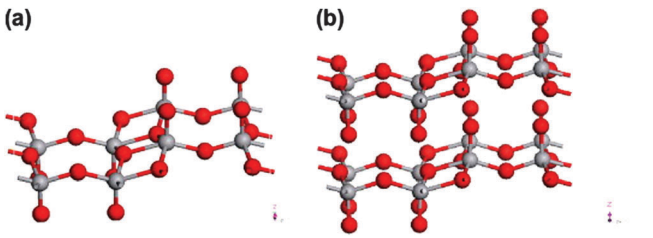

Fig. 21 Optimized geometries of the $V_2O_5(001)$ surface: (a) the $1 \times 2 \times 1$ surface cell and (b) the $2 \times 2 \times 1$ surface cell. The red spheres denote oxygen, and the gray ones denote vanadium.[30]

The adsorption of Hg^0 is stronger than that of HCl, so the oxidation reaction is initiated more favorably by Hg^0 adsorbing on the $V_2O_5(001)$ surface, and the adsorbed Hg forms $Hg_{(ads)}$ over the catalytic surface. $Hg_{(ads)}$ reacts fairly rapidly with chlorine species to form surface HgCl, and then reacts with chlorine species to form surface $HgCl_2$; finally $HgCl_2$ desorbs from the V_2O_5 surface.

The SCR catalyst with a tetrahedrally coordinated divanadate unit supported on a 3-layer $TiO_2(001)$ slab is modeled to represent a catalyst with low vanadia loadings.[27] Plane-wave DFT calculations with the GGA-PBE functional were carried out, and adsorption energy suggests a negligible interaction between Hg with the vanadia dimer. HCl and HgCl adsorb more strongly than Hg, and HgCl has a cooperative effect on the HCl adsorption. Fig. 22 shows the oxidized mechanism of mercury on the V_2O_5–TiO_2 SCR catalyst. HgCl is formed following an E–R mechanism where gas phase Hg interacts with adsorbed HCl due to the weak Hg adsorption energies. A L–H mechanism is proposed due to the stronger HCl and HgCl interaction with the surface, and the higher concentration of HCl in the gas phase compared to Hg, both of which make the adsorption of HCl on surface O more probable than the interaction of the surface with Hg. This is good in line with the results reported by He *et al.* and Eom *et al.*[14,128] However, a kinetic model is lacking to illustrate this mechanism, and the activation energy of every step and rate-determining step has not been obtained. In addition, under flue gas conditions, water coverage is temperature-dependent. Adsorbed water acts as a Lewis base, donating electrons to the $TiO_2(001)$ surface support, which increases the negative charge and reactivity of the oxygen atoms of the vanadia dimer. Therefore, the surface having H_2O adsorbed on a neighboring oxygen atom increases the adsorption energies of Hg and HCl, respectively. The effect of another active phase WO_3 on the V_2O_5–TiO_2 SCR catalyst has also been studied by using the same method and parameters with Hg^0 oxidizing on the vanadia supported on 3-layer $TiO_2(001)$ slab.[28] The adsorption energy, the Bader charge and PDOS have been calculated, and it can be concluded that the adsorption energies of Hg, Cl, HCl and HgCl on the binary monolayer systems (100% V_2O_5–TiO_2 or 100% WO_3–TiO_2) are higher than that of the ternary systems (V_2O_5–WO_3–TiO_2 with different V_2O_5/WO_3 ratios), which shows that the latter has a higher reactivity.

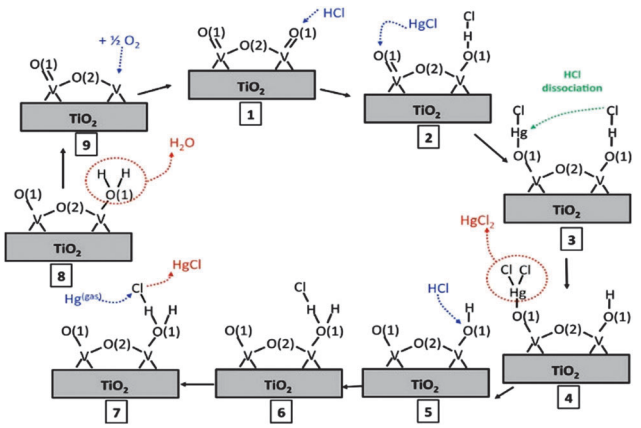

Fig. 22 Proposed mechanism of mercury oxidation on the vanadia–titania SCR catalyst. Blue arrows indicate an adsorption step, green arrows indicate a dissociation step, and red arrows indicate a desorption step.[27]

Fe_2O_3 exhibits significant catalytic effects in the oxidation of Hg^0, and a large amount of Hg^{2+} has been formed in the presence of Fe_2O_3.[96] α-Fe_2O_3 and γ-Fe_2O_3 both show effective oxidization capacity, and therefore remove Hg.[98] It is known that Hg^0 reacts with chlorine species to form Hg^+ and Hg^{2+} in coal combustion flue gas, and mercury chloride is assumed to be the dominant form of oxide (Hg^{2+}) species.[130] In addition, the presence of H_2S and O_2 can also influence the oxidation of Hg^0.[131,132] The co-adsorption of H_2S and Hg on the α-$Fe_2O_3(001)$ surface was discussed at the GGA-PBE level in CASTEP, and the L–H and E–R mechanisms are considered to explore the Hg^0 oxidization mechanism by H_2S.[31] Hg^0 and H_2S was simultaneously placed on the α-$Fe_2O_3(001)$ surface with different original configurations. After optimization, Hg^0 remained on the surface and interacted with the Fe atom, whereas H_2S separated from the substrate. And a huge repulsive force was produced between Hg^0 and H_2S during the optimization process, which shows that the existence of H_2S not only weakened Hg^0 adsorption, but also restrained its behavior. So the L–H mechanism is not possible for the oxidization of Hg^0. The E–R mechanism with Hg^0 adsorption on the H_2S/α-Fe_2O_3 surface was verified as the only possible mechanism behind the reaction process, where H_2S is firstly dissociated in two steps, *i.e.*, $H_2S \rightarrow HS + H$ and $HS \rightarrow S + H$ by the catalytic effect of α-Fe_2O_3. The adsorbed sulfur reacts with gaseous Hg^0 to form HgS. In addition, a series of adsorption experiments has been carried out to verify the mechanism.[133] H_2S and Fe_2O_3 are both indispensable factors for the high removal efficiency of Hg^0, and Fe_2O_3 behaves much more actively in Hg^0 adsorption under the influence of H_2S. Hg adsorption experiments on H_2S pre-adsorbed α-Fe_2O_3 shows that H_2S can be adsorbed on the surface of Fe_2O_3, and the adsorbed H_2S plays a dominant role in subsequent Hg^0 removal, which is in good agreement with the results of theoretical calculations.

O_2 can also promote the adsorption and oxidation of Hg^0 to a certain extent,[134] and can easily and efficiently be adsorbed on α-Fe_2O_3.[135] So the adsorption of Hg^0 on the O_2 embedded α-$Fe_2O_3(001)$ surface has been investigated at the GGA-PBE level to clarify the effect of O_2 on the capture of mercury by α-Fe_2O_3.[136] Previous experiments[137] show that Hg^0 could be

Table 9 The optimized parameters of Hg^0 adsorption on substrates for various coverage degrees[136]

Coverage	E_{ads} (eV)	R_{O-Hg} (Å)	R_{O-Fe} (Å)
0.25	−0.78	2.22	1.91
0.5	−2.20	2.03/2.04	1.95/1.97
0.75	−2.45	2.08/2.06/2.10	1.85/1.91/1.87
1-I	−2.78	2.16/2.31/2.22/4.99	1.81/1.83/1.89/1.92
1-II	−2.26	2.09/2.09/2.59/4.56	1.69/2.00/1.88/1.81

oxidized by the active oxygen atom on the surface of nano-Fe_2O_3, as well as lattice oxygen in nano-Fe_2O_3. However, Hg^0 prefers to adsorb on the α-Fe_2O_3(001) surface with the Fe atom, so the oxidization of Hg^0 by lattice oxygen has not been considered. Table 9 shows the optimized parameters of Hg^0 adsorption on substrates for various coverage degrees. The adsorption energy of −0.78 eV at 0.25 ML O coverage implies that the adsorption mechanism of Hg^0 on the O/α-Fe_2O_3(001) surface belongs to weak chemisorption. In addition, the oxygen coverage significantly influences the adsorption of Hg^0. The adsorption of Hg^0 on the surface changes from weak chemisorption into stronger chemisorption as the O coverage increases from 0.25 to 1 ML, demonstrating that higher coverage of the O atom may promote Hg^0 removal.

Zinc oxide (ZnO) is the most widely used agent to remove sulfur species such as H_2S from gas streams, due to the negative effects of H_2S on the environment and chemical processing.[138–141] The emission of mercury (Hg) in coal has also attracted growing attention due to its large impact on the environment and human health.[127,142] The experimental results show that sulfur can improve the removal of Hg using different materials.[143,144] And the HgS(s) formed is relatively insoluble and less volatile than Hg^0, and thus less harmful.[145] In our previous work,[37] the adsorptions of Hg-containing species on the ZnO(10$\bar{1}$0) surface were studied by using the DFT method with the GGA-PW91 functional in Dmol^3. Elemental Hg is weakly adsorbed on the ZnO(10$\bar{1}$0) surface with an adsorption energy of 0.28 eV, and PDOS (Fig. 23) shows that only s and p states slightly broaden and the sharp peak of the d state of the Hg atom is not changed before and after adsorption, indicating weak interaction between the Hg atom and the surface. HgS is strongly bound to the surface with an adsorption energy of 2.34 eV, which implies that the oxidized form of mercury is favored for removing mercury from flue gas. Therefore, the oxidation mechanism of elemental Hg to HgS has also been investigated. The potential energy diagram shows that the dissociation of H_2S is hardly influenced by the adsorbed Hg atom. The E–R and L–H mechanisms are considered and shown in Fig. 24. The kinetics analysis shows that the dissociated S on the surface can easily capture Hg^0, leading to the formation of HgS with activation energies of 0.01 and 0.54 eV for L–H and E–R mechanisms, respectively. So it can be concluded that ZnO can efficiently remove Hg^0 in flue gas under an atmosphere of H_2S. In addition, the role of oxygen defect on the ZnO(10$\bar{1}$0) surface has been investigated, and shows that it does not have a significant effect on the adsorption of Hg^0, while it enhances the adsorption of HgS. However, the activation energy for the formation of HgS on the oxygen-vacancy surface is higher than that on the perfect surface, which shows that the oxygen defect on the ZnO(10$\bar{1}$0) surface has an negative effect on mercury removal.

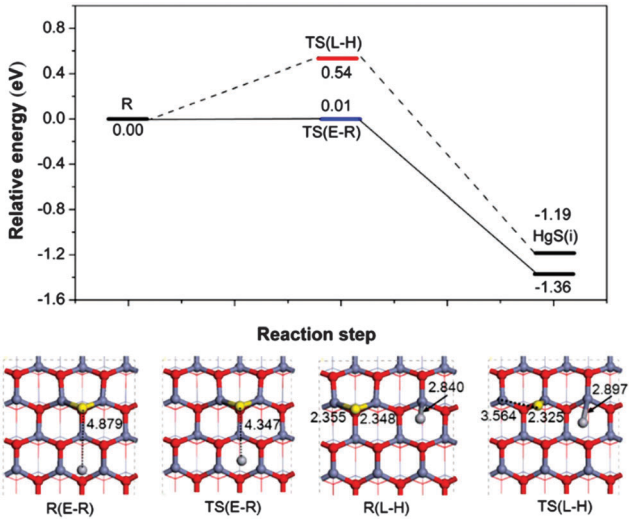

Fig. 24 The potential energy diagram for the formation of the HgS *via* E–R and L–H mechanisms and the corresponding structures.[37]

In addition, Cl_2 or HCl is also an effective oxidant to oxidize Hg^0, leading to the formation of $HgCl_2$,[146–149] which is generally thought to be the main oxide in coal-derived flue gas, and which is slightly less volatile and better water-soluble than Hg^0.[150] The adsorptions of Cl_2, HCl, HgCl and $HgCl_2$ are studied first; from these investigations it can be concluded that Cl_2 and HCl are dissociatively adsorbed on the surface, and the Cl atom binds to two adjacent Zn atoms. HgCl primarily exists in dissociative mode, and only trace amounts of HgCl existing in molecular mode explains why the concentration of HgCl cannot be measured directly using experiments.[151,152] It implies that HgCl is not a stable intermediate during Hg^0 oxidation by Cl_2 or HCl on the ZnO(10$\bar{1}$0) surface. $HgCl_2$ is strongly adsorbed on the surface in the molecular mode, which indicates that the oxidation of Hg^0 is necessary for its removal from flue gas. Three Hg^0 oxidation mechanisms have been investigated by employing the Dmol^3 package with the GGA-PW91 functional (Fig. 25), and $HgCl_2$ is easily formed *via* both the E–R and L–H mechanisms, with activation energies of 0.04 and 0.55 eV, respectively, while the M–M mechanism is unfavorable, since a high activation energy of 2.86 eV is needed for Hg^0 reacting with the lattice oxygen of ZnO. In addition, the

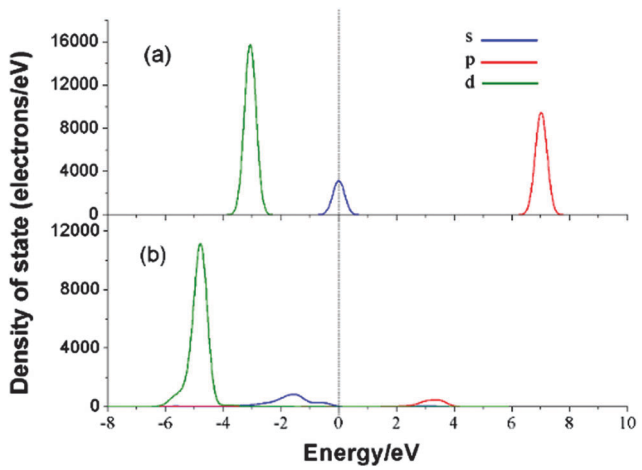

Fig. 23 PDOS analysis of the Hg atom before and after adsorption on the ZnO(10$\bar{1}$0) surface. (a) The free Hg atom and (b) the adsorbed Hg atom.[37]

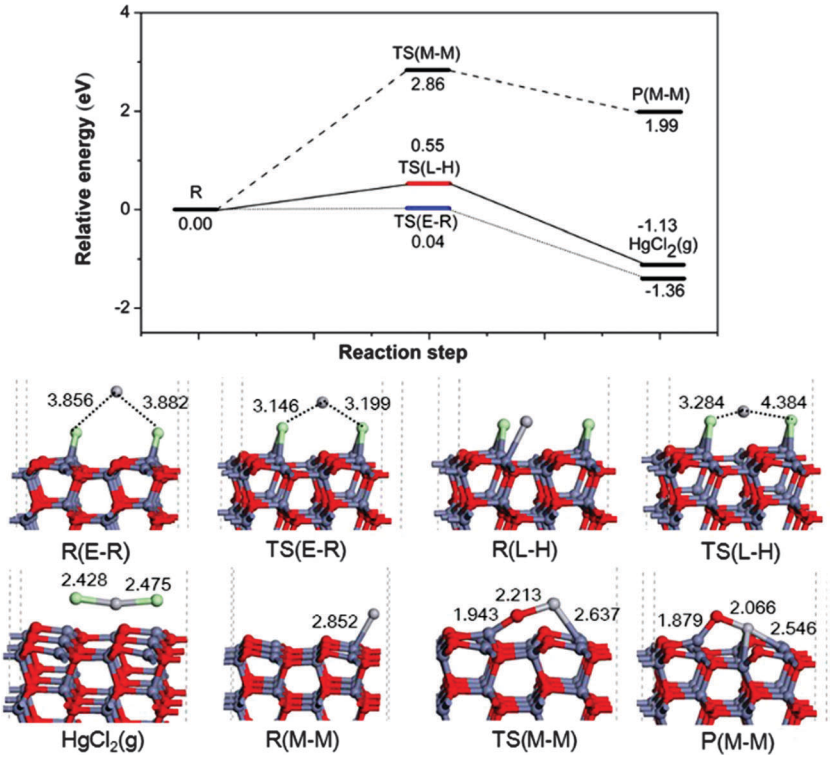

Fig. 25 Potential energy diagram for the oxidation pathway of Hg^0 by Cl_2 on the ZnO surface.[36]

influence of H dissociated by HCl on the formation of $HgCl_2$ has also been considered. It is unfortunate that $HgCl_2$ is not formed on the surface when the adsorbed H atoms are present, showing that the presence of H is disadvantageous to Hg^0 oxidation and inhibits the formation of $HgCl_2$. So Cl_2 is the primary Cl-containing species responsible for Hg^0 oxidation on the ZnO surface.[36] A similar result has been obtained using an experimental study of Hg^0 removal by Fe_2O_3 in the presence of HCl.[153,154] However, HCl is an effective flue gas component for Hg^0 oxidation over the CeTi catalyst, which can be adsorbed and reacted with the catalyst to form active oxychloride. And then, the active surface species react with adsorbed Hg^0 leading to $HgCl_2$ *via* the HgCl intermediate using the L–H mechanism.[155] On the Au(111) surface, the H atom from HCl dissociation consumes the electron charge of the gold atoms, and lowers the strength of interaction between the gold atoms and the reaction intermediates. Eventually HCl enhances the Hg oxidation reaction by lowering the activation energy for the formation of HgCl and $HgCl_2$.[24] The situation on the ZnO($10\bar{1}0$) surface is different. The charge of 0.132 *e* transfers from H atoms to the surface during dissociative adsorption of HCl on the surface, thereby strengthening the interaction between the adsorbed Cl atom and the surface, which ultimately inhibits the Hg^0 oxidation.

Copper based sorbents are widely used to control mercury emissions in coal-fired flue gas. CuO nanoparticles were dispersed on a quartz filter placed in an oxidation reactor to oxidize Hg^0 to Hg^{2+} at low HCl concentrations.[156] CuO_x impregnated on neutral Al_2O_3 sorbents were found to enhance the catalytic oxidation of elemental mercury in the presence of hydrogen chloride (HCl).[157] The Hg^0 vapor was mostly oxidized by sorbents in the presence of relatively high concentrations of HCl due to the formed active chlorine. As the HCl concentration increases, the mercury oxidation rate increases as well. The Hg^0 oxidation rates also increased with increasing temperature. In addition, the oxidation mechanism of Hg^0 has been studied, which shows that the first step is the hydrogen abstraction from HCl, leading to active chlorine and hydroxyl species. Then, Hg^0 can be oxidized by the active chlorine species. The chlorine atoms are supplied by hydrogen chloride, so a high concentration of HCl can promote the mercury removal process. CuO_x species act as catalysts *via* the redox shift between Cu^{2+} and Cu^+. Higher temperatures accelerate the Cl release step. Consequently, the mercury oxidation mechanism of the sorbents is proposed to follow the M–M mechanism:

$$Cu^{2+} + O^{2-} + HCl \leftrightarrow Cu^{+} + Cl^{-} + OH^{-} \quad (R13)$$

$$Cu^{+} + O^{2-} + HCl \leftrightarrow Cu^{0} + Cl^{-} + OH^{-} \quad (R14)$$

$$Cu^{+} + O_2 \leftrightarrow Cu^{2+} + O^{2-} \quad (R15)$$

$$OH^{-} + OH^{-} \leftrightarrow H_2O + O^{2-} \quad (R16)$$

$$Hg^0 + Cl^{-} \leftrightarrow HgCl^{-} \quad (R17)$$

$$HgCl^{-} + Cl^{-} + e^{-} \leftrightarrow HgCl_2 \quad (R18)$$

$$HgCl_{2(g)} \leftrightarrow HgCl_{2(ad)} \quad (R19)$$

$$\text{Total reaction: } Hg + 2HCl + 1/2O_2 \leftrightarrow HgCl_2 + H_2O \quad (R20)$$

Recently, the adsorption and oxidation of Hg by Cl-containing species in flue gas on the CuO(111) surface (Fig. 26) have been

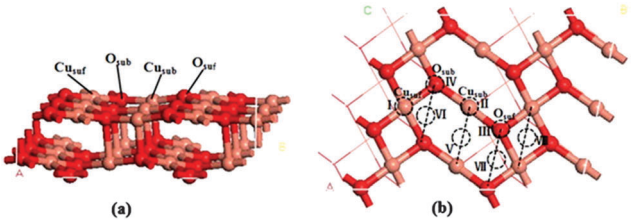

Fig. 26 The slab model of the CuO(111) surface. (a) Side view; (b) top view. The Cu and O atoms are in orange and red, respectively.[35]

investigated by using the DFT method with the GGA-PW91 functional in the Dmol^3 package.[35] A weakly physisorbed mode is obtained for the Hg atom on the CuO(111) surface with an adsorption energy of 0.28 eV. The mercury oxidation reaction of Hg^0 on the CuO(111) surface *via* Cl_2 and HCl is examined. Cl dissociated from HCl or Cl_2 prefers surface Cu, and the Hg atom in gas approaches the surface Cl atoms, leading to the formation of $HgCl_2$ *via* the E–R mechanism. The activation energies are 0.15 and 0.03 eV for Cl_2 and HCl as oxidants (Fig. 27), respectively. So the authors believe that the oxidation reaction of Hg^0 *via* HCl on the CuO(111) surface is likely the dominant interaction pathway. In our opinion, Hg can be easily oxidized by Cl_2 and HCl over the CuO catalyst due to both the low energy barriers.

Copper cobaltite, with general formula $Cu_xCo_{3-x}O_4$, is selected to control the emission of Hg^0 from the combustion process owing its oxidation capacity.[158] $Cu_{1.5}Co_{1.5}O_4$ showed the best Hg^0 oxidation ability, and the product is HgO. In addition, the SO_2 anti-poisoning ability of $Cu_xCo_{3-x}O_4$ increased with a

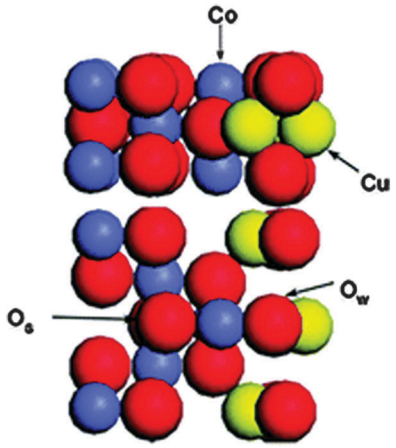

Fig. 28 The notation of atoms in the $CuCo_2O_4$(110) slab and the illustration of two orientations of the $CuCo_2O_4$(110) slab. The upper $CuCo_2O_4$(110) slab is the top view, and the below is the side view.[38]

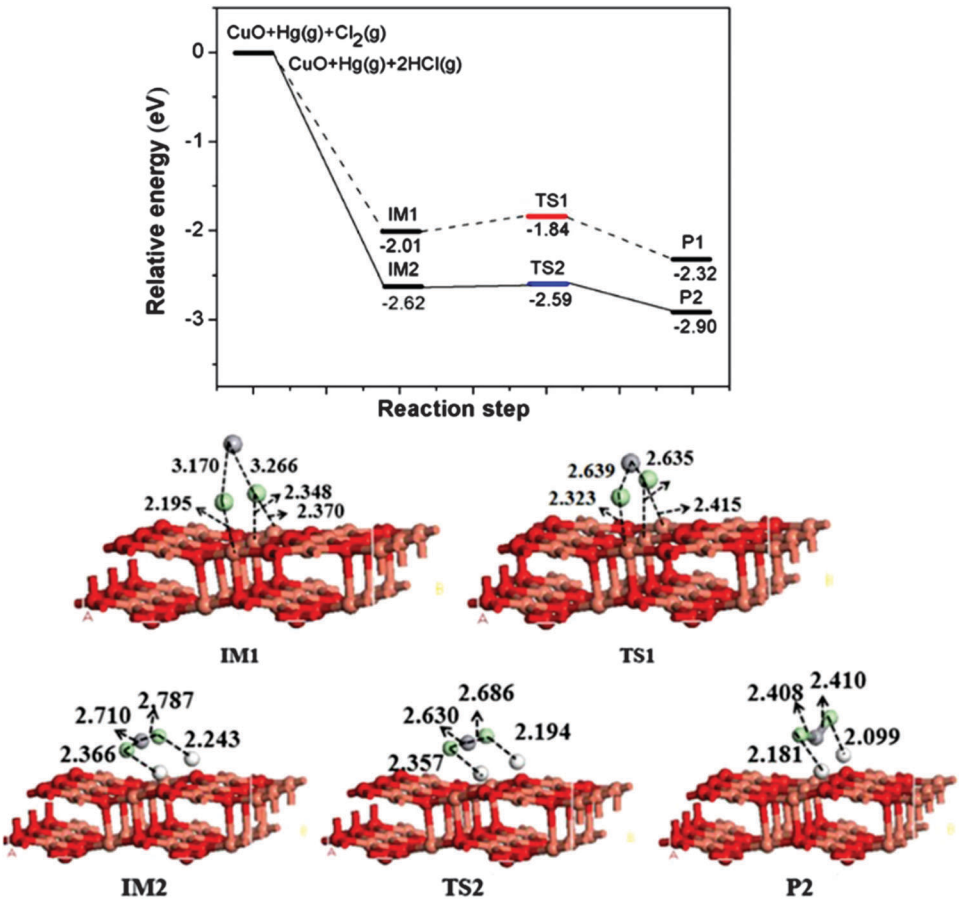

Fig. 27 Energy profile of the reaction pathway of Hg^0 oxidation by Cl_2 and HCl on the CuO(111) surface and the structures of related intermediates, transition states and final states.[35]

continuous increase of x from 0.75 to 2.25. Therefore, the periodic $CuCo_2O_4(110)$ surface using the four-layer and $p(2 \times 2)$ model has been built (Fig. 28), and different N doped $CuCo_2O_4(110)$ surfaces have also been built. All calculations were performed in CASTEP with the GGA-PBE functional.[38] In fact, DFT + U should be used in this strongly correlated material. The mercury oxidation/chemical adsorption on these surfaces is studied. On the perfect surface, Hg is physically adsorbed on the surface with an exothermicity of −0.25 eV. And then, the Hg atom migrates to O_w or O_s *via* $(Hg–O_w)_{TS}$ or $(Hg–O_s)_{TS}$, with energy barriers of 0.85 or 1.83 eV, respectively. In addition, the activation energy for the reverse reaction from IM1 to $(Hg–O_w)_{TS}$ is higher than the other path (Fig. 29), which shows that intermediate M1 is more stable than the intermediate involving O_s. The first step is also the rate-determining step. On the different N doped surfaces, 3N doped $CuCo_2O_4(110)$ may not exist due to its thermodynamic instability. There are lower activation energies on the 2N doped surface than that on the 1N doped surface. On the 2N doped surface, there are two paths for Hg oxidation or chemical adsorption, as shown in Fig. 30. The reaction on the $CuCoO_4–N_{bs}(110)$ surface is not the most favorable reaction pathway due to its highest substitution energy, and the other path on the $CuCoO_4–N_{bb}(110)$ surface involving O_w is favorable with an activation energy of 0.69 eV. It can be concluded that N-doping can increase the activity of surface O bonded with one Cu^{2+} ion and one Co^{3+} ion (O_w),

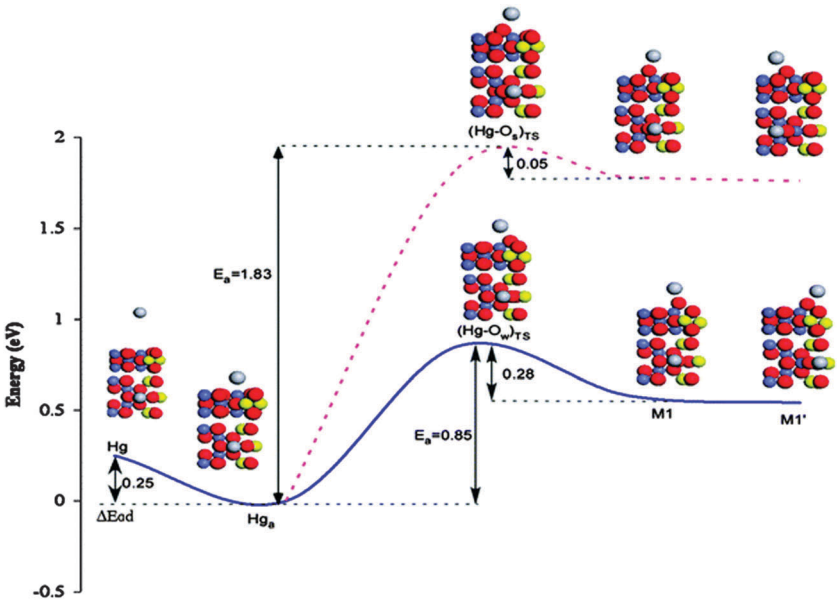

Fig. 29 Reaction pathways of Hg oxidation on the perfect $CuCo_2O_4(110)$ surface.[38]

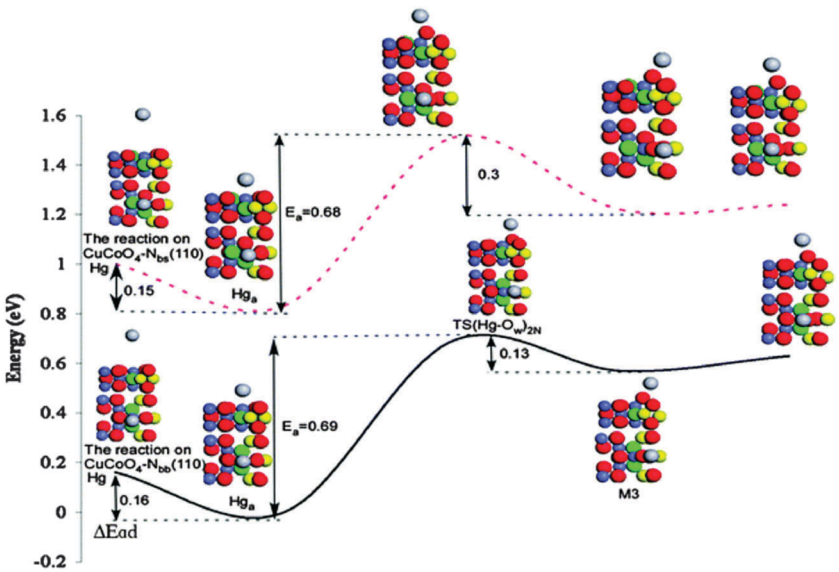

Fig. 30 Reaction pathways of Hg oxidation/chemical adsorption on different 2N doped $CuCo_2O_4(110)$ surfaces.[38]

which is in line with the previous experiment.[159] N atoms have been doped into the crystal lattice of $CuCoO_4$ by XRD and XPS analysis, and shows no adverse effect on both Co^{3+} or Cu^{2+} octahedral cation structure of $CuCoO_4$, and are responsible for the significant enhancement in Hg^0 oxidation ability of $CuCoO_4$ impregnated NH_4Cl or NH_4Br.

The effect of different flue gases on the removal of Hg has been investigated in the experiment. SO_2 has not been oxidized to increase sulfuric acid concentrations in the flue gas over the mercury oxidation SCR catalyst, and very little NO has been oxidized to NO_2. These are both positive results for removing Hg.[160] The CuO–MnO_2–Fe_2O_3/γ-Al_2O_3 catalyst was prepared for gas-phase mercury oxidation, which yielded more than 70% oxidation efficiency using a simulated flue gas (O_2, CO_2, HCl, NO, SO_2, H_2O and balanced with N_2).[161] Without O_2, the presence of HCl inhibited Hg^0 adsorption and subsequent oxidation due to the competition for active sites between HCl and Hg^0 on the catalyst surface. The E–R mechanism was proposed to explain the heterogeneous Hg^0 oxidation. HCl adsorbed on the catalyst surface was first oxidized to active Cl species by O_2. Then the active Cl would react with gas-phase or weakly bonded Hg^0 to produce $HgCl_2$, which can be shown as follows:

$$4HCl_{(g)} + O_2 \rightarrow 2H_2O + 4Cl^*_{(ad)} \quad (R21)$$

$$Hg^*_{(g)} + Cl^*_{(ad)} \rightarrow HgCl_{(ad)} \quad (R22)$$

$$HgCl_{(ad)} + Cl^*_{(ad)} \rightarrow HgCl_{2(ad)} \quad (R23)$$

$$HgCl_{2(ad)} \rightarrow HgCl_{2(g)} \quad (R24)$$

SO_2 had little effect on Hg^0 oxidation without O_2, however, the combination of O_2 and SO_2 could promote the Hg^0 oxidation because the oxidation properties were enhanced after the catalyst was sulfated. The reactions are proposed as follows:[162]

$$SO_2 + O_{lattice} \rightarrow SO_3 \quad (R25)$$

$$2Hg^0 + SO_3 \rightarrow Hg_2SO_3 \quad (R26)$$

$$SO_2 + 1/2O_2 \rightarrow SO_3 \quad (R27)$$

$$Hg^0 + SO_3 + 1/2O_2 \rightarrow HgSO_4 \quad (R28)$$

NO promoted Hg^0 oxidation due to the formation of multi-activity NO_x species with and without O_2, resulting in enhanced Hg^0 oxidation, and further formation of $Hg(NO_3)_2$. The pathway is shown as follow:

$$NO + O_{lattice} \rightarrow NO_2 \quad (R29)$$

$$NO + 1/2O_2 \rightarrow NO_2 \quad (R30)$$

$$Hg^0 + NO_2 \rightarrow HgO + NO \quad (R31)$$

$$Hg^0 + NO_2 + O_2 \rightarrow Hg(NO_3)_2 \quad (R32)$$

NH_3 would inhibit Hg^0 oxidation, but once NH_3 was cut off, the efficiency fully recovered.

3.2.3 Other catalysts. HZSM-5-supported Fe and Cu have been synthesized, and the efficiency of removal of mercury has also been determined.[163,164] Fe/HZSM-5 and Cu/HZSM-5 possessed a strong ability for Hg^0 removal. O_2 can promote Hg^0 oxidation while SO_2 inhibits Hg^0 oxidation. The product is probably adsorbed $HgCl_2$ below 200 °C over the Fe/HZSM-5 catalyst, and the product might be both adsorbed and gaseous $HgCl_2$ above 200 °C. For the Cu/HZSM-5 catalyst, the Hg^0 removal efficiency enhanced and then decreased with the increase of reaction temperature. HZSM-5 modified by CeO_2 has also been prepared. The acidic sites of HZSM-5 could effectively adsorb Hg^0 from the flue gas, and CeO_2 promotes the oxidation of adsorbed Hg^0.[165] The optimal loading is 6%, and which has high Hg^0 removal efficiency at a reaction temperature below 300 °C. Additionally, the presence of H_2O has an adverse effect on Hg^0 removal, while O_2 can promote the removal efficiency of NO and SO_2 for Hg^0. Besides, the reduced metal oxides can be reoxidized by O_2, and the lattice oxygen replenished, therefore, the high chemisorbed sites on the CeO_2/HZSM-5 are maintained. The possible mechanisms are shown as follow:

$$Hg^0_{(g)} + HZSM\text{-}5 \leftrightarrow Hg^0_{(ad)} \quad (R33)$$

$$Hg^0_{(g)} + HZSM\text{-}5 \leftrightarrow Hg^0_{(ad)} \quad (R34)$$

$$Hg^0_{(ad)} + 2CeO_2 \rightarrow HgO_{(ad)} + Ce_2O_3 \quad (R35)$$

$$2Ce_2O_3 + O_2 \rightarrow 4CeO_2 \quad (R36)$$

$$2NO_{(g)} + O_2 \xrightarrow{CeO_2} 2NO_{2(ad)} \quad (R37)$$

$$2SO_2(g) + O_2 \xrightarrow{CeO_2} 2SO_{3(ad)} \quad (R38)$$

$$NO_{2(ad)} + Hg_{(ad)} \rightarrow NO + HgO_{(ad)} \quad (R39)$$

$$SO_{3(ad)} + Hg_{(ad)} \rightarrow SO_2 + HgO_{(ad)} \quad (R40)$$

$$SO_{3(ad)} + Hg_{(ad)} \rightarrow HgSO_{4(ad)} \quad (R41)$$

Although there is no theoretical study on the adsorption and oxidation of Hg over the zeolite catalyst. It is worth noting that gaseous molecules are generally dispersed in the zeolite channels as a monolayer dispersion during their adsorption,[166] and an accurate description of weak intermolecular interactions is necessary because the conventional DFT method cannot provide reliable results for this interaction.[167,168] Many correction methods have been developed,[169–172] among them are widely used Grimme's dispersion correction ones.[173–175] The DFT with dispersion correction (DFT-D2) method has been used to study adsorption and dimerization of propene to C6 species inside the main channel of zeolite SAPO-5, resulting from the substitution a P atom with a Si atom in $AlPO_4$-5.[176] The crystallization thermochemistry, structure stabilities and acid properties of B-, Al, and Ga-incorporated H-, NH_4-, Li-, Na- and K-forms MTW zeolites have also been studied using the DFT-D2 method.[177]

3.2.4 Comparison of different mercury removal technologies. The oxidation mechanisms of Hg^0 on different catalyst surfaces have been studied by using the DFT method; the different software and functionals, the energy barriers and the possible mechanisms are listed in Table 10. On these surfaces, the lowest barrier is only 0.01 eV when S is doped on the ZnO($10\bar{1}0$) surface *via* the E–R mechanism, while the highest barrier is 3.12 eV when S is on the O-vacancy ZnO($10\bar{1}0$) surface *via* the E–R

Table 10 The energy barriers and the possible mechanisms of Hg^0 oxidation with different oxidants on the different surfaces

Surfaces	Software and functional	Oxidants	E_a (eV)	Mechanism
Au(111)[24]	VASP, GGA-PW91	Cl_2	0.22	—
		HCl	0.14	—
Defect Au(111)[24]	VASP, GGA-PW91	Cl_2	0.52	—
		HCl	0.22	—
Pd(100)[29]	CASTEP, GGA-PBE	HCl	0.66	L–H
α-Fe_2O_3(001)[31]	CASTEP, GGA-PBE	H_2S	—	E–R
V_2O_5[27]	VASP, GGA-PBE	HCl	—	L–H
ZnO(10$\bar{1}$0)[36]	Dmol^3, GGA-PW91	Cl_2	0.55	L–H
			0.04	E–R
			2.86	M–M
ZnO(10$\bar{1}$0)[37]	Dmol^3, GGA-PW91	S	0.54	L–H
			0.01	E–R
O-vacancy ZnO(10$\bar{1}$0)[37]	Dmol^3, GGA-PW91	S	2.54	L–H
			3.12	E–R
CuO[35]	Dmol^3, GGA-PW91	Cl_2	0.17	E–R
		HCl	0.03	E–R

mechanism due to S filling into the O vacancy site. It infers that the surface defect has an adverse effect on the oxidation of Hg^0; similar results have been obtained on the Au(111) surface, and the defect on the surface also suppresses the oxidation of Hg^0. However, the effect of defects on the other surface upon the Hg^0 oxidation is lacking. In addition, the kinetic parameters have not been obtained for Hg^0 oxidation on some catalyst surfaces, which results in difficulties in comparison with different catalysts. Focused on the reaction of Hg^0 oxidizing to $HgCl_2$ by Cl_2, the activation energies with catalysts are lower than that without catalysts at different theoretical levels,[48] which implies that the oxidation reaction can be effectively accelerated.

4. Conclusions

The understanding of adsorption and oxidation of mercury has been improved through studies using computational chemistry methods. However, these theoretical studies are mainly based on the experimental results, especially for choosing research materials, and prediction of new materials according to the theoretical results is lacking. We believe that computational chemistry can quickly guide experiments towards promising sorbent materials.

In previous work, some oxidation kinetics data are lacking; these can provide a more detailed and deep understanding of the activity of catalysts. In addition, the theoretical results are obtained by different methods or parameters, which results in difficulty in comparing the properties for different materials, so a systemic study is needed.

Notably, the current models have been built according to the main active metal or metal oxides. In fact, the support plays an important role in mercury removal, which not only disperses the active constituent, but also works with the active constituent *via* the coordination effect. In addition, defects on the surface also have a significant influence on the properties of catalysts, some of which can promote mercury removal, but some of which decrease the removal mercury ability. For future studies, the effect of support, and different surface defects on the mercury oxidation should be considered.

Furthermore, the mercury removal capacity of different materials will be influenced by different gases in the atmosphere, including CO, H_2, O_2, NO and SO_2, some of which can promote mercury removal, but some can also inhibit removal ability. In the future, the effect of real flue gases on the adsorption and oxidation of Hg should be investigated by using the theoretical calculation method.

Last but not least, activated carbon is with large surface area, and is widely used to be as a supporter. Metals or metal oxides can effectively catalyze the dissociation of HCl, Cl_2 and H_2S to provide activated oxidant, thereby promoting the oxidation of Hg^0. However, metals with high Hg removal efficiency are generally noble metals. Therefore, metal oxides loading on activated carbon materials may be a promising research in theory and experiment, which can combine the advantages of these two materials. And both high removal efficiency of Hg and low cost are considerable.

Acknowledgements

We gratefully acknowledge the National Younger Natural Science Foundation of China (Grant No. 21103120), Program for the Innovative Talents of Higher Learning Institutions of Shanxi, the State Key Laboratory of Fine Chemicals (KF1205) and Wyoming Engineering Initiative in the U.S.

References

1 A. Franco and A. R. Diaz, *Energy*, 2009, **34**, 348–354.
2 J. M. Beér, *Prog. Energy Combust. Sci.*, 2000, **26**, 301–327.
3 A. Demirbaş, *Energy Convers. Manage.*, 2003, **44**, 1465–1479.
4 J. H. Pavlish, E. A. Sondreal, M. D. Mann, E. S. Olson, K. C. Galbreath, D. L. Laudal and S. A. Benson, *Fuel Process. Technol.*, 2003, **82**, 89–165.
5 S. D. Serre and G. D. Silcox, *Ind. Eng. Chem. Res.*, 2000, **39**, 1723–1730.
6 R. A. Monterrozo, M. Fan and M. D. Argyle, *J. Environ. Eng.*, 2012, **138**, 386–391.
7 E. G. Pacyna, J. M. Pacyna, J. Fudala, E. Strzelecka-Jastrzab, S. Hlawiczka and D. Panasiuk, *Sci. Total Environ.*, 2006, **370**, 147–156.
8 E. G. Pacyna, J. M. Pacyna, K. Sundseth, J. Munthe, K. Kindbom, S. Wilson, F. Steenhuisen and P. Maxson, *Atmos. Environ.*, 2010, **44**, 2487–2499.
9 U. S. E. P. Agency, Mercury News, http://www.epa.gov/hg/.
10 K. C. Galbreath and C. J. Zygarlicke, *Environ. Sci. Technol.*, 1996, **30**, 2421–2426.
11 A. A. Presto and E. J. Granite, *Environ. Sci. Technol.*, 2006, **40**, 5601–5609.
12 S. Yang, Y. Guo, N. Yan, D. Wu, H. He, Z. Qu, C. Yang, Q. Zhou and J. Jia, *ACS Appl. Mater. Interfaces*, 2011, **3**, 209–217.

13 S. Kellie, Y. Cao, Y. Duan, L. Li, P. Chu, A. Mehta, R. Carty, J. T. Riley and W.-P. Pan, *Energy Fuels*, 2005, **19**, 800–806.
14 Y. Eom, S. H. Jeon, T. A. Ngo, J. Kim and T. G. Lee, *Catal. Lett.*, 2008, **121**, 219–225.
15 C.-X. Hu, J.-S. Zhou, Z.-Y. Luo, H. Sheng, G.-K. Wang and K.-F. Cen, *J. Environ. Sci.*, 2006, **18**, 1161–1166.
16 D. Mergler, H. A. Anderson, L. H. Man Chan, K. R. Mahaffey, M. Murray, M. Sakamoto and A. H. Stern, *AMBIO*, 2007, **36**, 3–11.
17 L. Jin, L. Zhang, Z. Li, J. M. Liu, R. Ye and A. Ren, *Reprod. Toxicol.*, 2013, **35**, 25–31.
18 G.-C. Fang, I. L. Yang and C.-K. Liu, *Atmos. Res.*, 2010, **97**, 97–105.
19 S.-J. Chen, C.-T. Lo, G.-C. Fang and C.-S. Huang, *Environ. Forensics*, 2012, **13**, 98–104.
20 J. Wilcox, E. Rupp, S. C. Ying, D.-H. Lim, A. S. Negreira, A. Kirchofer, F. Feng and K. Lee, *Int. J. Coal Geol.*, 2012, **90–91**, 4–20.
21 B.-A. Dranga, L. Lazar and H. Koeser, *Catalysts*, 2012, **2**, 139–170.
22 Y. Gao, Z. Zhang, J. Wu, L. Duan, A. Umar, L. Sun, Z. Guo and Q. Wang, *Environ. Sci. Technol.*, 2013, **47**, 10813–10823.
23 D. H. Lim, S. Aboud and J. Wilcox, *Environ. Sci. Technol.*, 2012, **46**, 7260–7266.
24 D. H. Lim and J. Wilcox, *Environ. Sci. Technol.*, 2013, **47**, 8515–8522.
25 S. Aboud, E. Sasmaz and J. Wilcox, *Main Group Chem.*, 2008, **7**, 205–215.
26 E. Sasmaz, S. Aboud and J. Wilcox, *J. Phys. Chem. C*, 2009, **113**, 7813–7820.
27 A. Suarez Negreira and J. Wilcox, *J. Phys. Chem. C*, 2013, **117**, 1761–1772.
28 A. Suarez Negreira and J. Wilcox, *J. Phys. Chem. C*, 2013, **117**, 24397–24406.
29 B. Zhang, J. Liu, J. Zhang, C. Zheng and M. Chang, *Chem. Eng. J.*, 2014, **237**, 344–351.
30 J. Liu, M. He, C. Zheng and M. Chang, *Proc. Combust. Inst.*, 2011, **33**, 2771–2777.
31 L. Tao, X. Guo and C. Zheng, *Proc. Combust. Inst.*, 2013, **34**, 2803–2810.
32 W. Xiang, J. Liu, M. Chang and C. Zheng, *Chem. Eng. J.*, 2012, **200–202**, 91–96.
33 S. Zhao, Z. H. Li, W. N. Wang, Z. P. Liu, K. N. Fan, Y. Xie and H. F. I. Schaefer, *J. Chem. Phys.*, 2006, **124**, 184102.
34 L. Geng, L. Han, W. Cen, J. Wang, L. Chang, D. Kong and G. Feng, *Appl. Surf. Sci.*, 2014, **321**, 30–37.
35 S. Sun, D. Zhang, C. Li, Y. Wang and Q. Yang, *Chem. Eng. J.*, 2014, **258**, 128–135.
36 L. Ling, S. Zhao, P. Han, B. Wang, R. Zhang and M. Fan, *Chem. Eng. J.*, 2014, **244**, 364–371.
37 L. Ling, P. Han, B. Wang and R. Zhang, *Chem. Eng. J.*, 2013, **231**, 388–396.
38 Z. Mei, M. Fan, R. Zhang, Z. Shen and W. Wang, *Phys. Chem. Chem. Phys.*, 2014, **16**, 13508–13516.
39 J. Wilcox, *J. Phys. Chem. A*, 2009, **113**, 6633–6639.
40 J. Wilcox, *Environ. Chem.*, 2011, **8**, 207–212.
41 A. Montoya, T. N. Truong and A. F. Sarofim, *J. Phys. Chem. A*, 2000, **104**, 8409–8417.
42 S. Niksa, J. J. Helble and N. Fujiwara, *Environ. Sci. Technol.*, 2001, **35**, 3701–3706.
43 J. Liu, W. Qu, J. Yuan, S. Wang, J. Qiu and C. Zheng, *Energy Fuels*, 2010, **24**, 117–122.
44 J. Wilcox and T. Okano, *Energy Fuels*, 2011, **25**, 1348–1356.
45 M. E. Goodsite, J. M. C. Plane and H. Skov, *Environ. Sci. Technol.*, 2004, **38**, 1772–1776.
46 B. Krishnakumar and J. J. Helble, *Fuel Process. Technol.*, 2012, **94**, 1–9.
47 J. Wilcox, *Mercury Control*, Wiley-VCH Verlag GmbH & Co. KGaA, 2014, DOI: 10.1002/9783527658787, ch. 24, pp. 389–412.
48 I. Auzmendi-Murua, A. Castillo and J. W. Bozzelli, *J. Phys. Chem. A*, 2014, **118**, 2959–2975.
49 N. B. Balabanov, B. C. Shepler and K. A. Peterson, *J. Phys. Chem. A*, 2005, **109**, 8765–8773.
50 E. S. Olson, S. J. Miller, R. K. Sharma, G. E. Dunham and S. A. Benson, *J. Hazard. Mater.*, 2000, **74**, 61–79.
51 E. J. Granite, H. W. Pennline and R. A. Hargis, *Ind. Eng. Chem. Res.*, 2000, **39**, 1020–1029.
52 B. Hall, P. Schager and J. Weesmaa, *Chemosphere*, 1995, **30**, 611–627.
53 A. Murakami, M. A. Uddin, R. Ochiai, E. Sasaoka and S. Wu, *Energy Fuels*, 2010, **24**, 4241–4249.
54 R. Ochiai, M. A. Uddin, E. Sasaoka and S. Wu, *Energy Fuels*, 2009, **23**, 4734–4739.
55 T. Morimoto, S. Wu, M. Azhar Uddin and E. Sasaoka, *Fuel*, 2005, **84**, 1968–1974.
56 H. Zhang, J. Zhao, Y. Fang, J. Huang and Y. Wang, *Energy Fuels*, 2012, **26**, 1629–1637.
57 B. Padak and J. Wilcox, *Carbon*, 2009, **47**, 2855–2864.
58 E. Sasmaz, A. Kirchofer, A. D. Jew, A. Saha, D. Abram, T. F. Jaramillo and J. Wilcox, *Fuel*, 2012, **99**, 188–196.
59 B. Padak, M. Brunetti, A. Lewis and J. Wilcox, *Environ. Prog.*, 2006, **25**, 319–326.
60 J. Liu, M. A. Cheney, F. Wu and M. Li, *J. Hazard. Mater.*, 2011, **186**, 108–113.
61 W. J. Stevens, M. Krauss, H. Basch and P. G. Jasien, *Can. J. Chem.*, 1992, **70**, 612–630.
62 S. B. Ghorishi, R. M. Keeney, S. D. Serre, B. K. Gullett and W. S. Jozewicz, *Environ. Sci. Technol.*, 2002, **36**, 4454–4459.
63 E. C. Rupp and J. Wilcox, *Fuel*, 2014, **117**, 351–353.
64 B. Van Otten, P. A. Buitrago, C. L. Senior and G. D. Silcox, *Energy Fuels*, 2011, **25**, 3530–3536.
65 S. Krishnan, B. K. Gullett and W. Jozewicz, *Environ. Sci. Technol.*, 1994, **28**, 1506–1512.
66 J. A. Korpiel and R. D. Vidic, *Environ. Sci. Technol.*, 1997, **31**, 2319–2325.
67 W. Liu, R. D. Vidic and T. D. Brown, *Environ. Sci. Technol.*, 2000, **34**, 154–159.
68 J. Liu, W. Qu, S. W. Joo and C. Zheng, *Chem. Eng. J.*, 2012, **184**, 163–167.
69 Y. Yao, V. Velpari and J. Economy, *Fuel*, 2014, **116**, 560–565.

70 J. Wang, J. Yang and Z. Liu, *Fuel Process. Technol.*, 2010, **91**, 676–680.
71 J. W. Wang, R. Q. Liu and X. J. Kong, *Adv. Mater. Res.*, 2012, **518–523**, 210–213.
72 J. W. Wang, J. L. Yang and Z. Y. Liu, *Adv. Mater. Res.*, 2012, **347–353**, 1847–1851.
73 X. Fan, C. Li, G. Zeng, Z. Gao, L. Chen, W. Zhang and H. Gao, *Energy Fuels*, 2010, **24**, 4250–4254.
74 X. Hua, J. Zhou, Q. Li, Z. Luo and K. Cen, *Energy Fuels*, 2010, **24**, 5426–5431.
75 C. M. Baldeck, G. W. Kalb and H. L. Crist, *Anal. Chem.*, 1974, **46**, 1500–1505.
76 D. B. Aeschliman and G. A. Norton, *Environ. Sci. Technol.*, 1999, **33**, 2278–2283.
77 S. A. Siddiqui, N. Bouarissa, T. Rasheed and M. S. Al-Assiri, *Mater. Res. Bull.*, 2013, **48**, 995–1002.
78 J. P. Perdew, K. Burke and Y. Wang, *Phys. Rev. B: Condens. Matter Mater. Phys.*, 1996, **54**, 16533.
79 P. J. Hay and W. R. Wadt, *J. Chem. Phys.*, 1985, **82**, 270–283.
80 P. J. Hay and W. R. Wadt, *J. Chem. Phys.*, 1985, **82**, 299–310.
81 W. R. Wadt and P. J. Hay, *J. Chem. Phys.*, 1985, **82**, 284–298.
82 T. Y. Yan, *Ind. Eng. Chem. Res.*, 1994, **33**, 3010–3014.
83 Y. Liu, D. J. Kelly, H. Yang, C. C. Lin, S. M. Kuznicki and Z. Xu, *Environ. Sci. Technol.*, 2008, **42**, 6205–6210.
84 L. Sun, A. Zhang, S. Su, H. Wang, J. Liu and J. Xiang, *Chem. Phys. Lett.*, 2011, **517**, 227–233.
85 P. Dowben, Y. Kime, C. Hutchings, W. Li and G. Vidali, *Surf. Sci.*, 1990, **230**, 113–122.
86 Y. Kime, J. Zhang and P. Dowben, *Surf. Sci.*, 1992, **268**, 98–112.
87 J. A. Steckel, *Phys. Rev. B: Condens. Matter Mater. Phys.*, 2008, **77**, 115412.
88 S. Poulston, E. J. Granite, H. W. Pennline, C. R. Myers, D. P. Stanko, H. Hamilton, L. Rowsell, A. W. J. Smith, T. Ilkenhans and W. Chu, *Fuel*, 2007, **86**, 2201–2203.
89 S. Affrossman and W. Erskine, *Trans. Faraday Soc.*, 1966, **62**, 2922–2927.
90 A. Jain, S. A. Seyed-Reihani, C. C. Fischer, D. J. Couling, G. Ceder and W. H. Green, *Chem. Eng. Sci.*, 2010, **65**, 3025–3033.
91 E. J. Granite, C. R. Myers, W. P. King, D. C. Stanko and H. W. Pennline, *Ind. Eng. Chem. Res.*, 2006, **45**, 4844–4848.
92 J. A. Hrdlicka, W. S. Seames, M. D. Mann, D. S. Muggli and C. A. Horabik, *Environ. Sci. Technol.*, 2008, **42**, 6677–6682.
93 J. Wang, H. Yu, L. Gen, J. Liu, L. Han, L. Chang, G. Gang and L. Ling, *Appl. Surf. Sci.*, 2015, DOI: 10.1016/j.apsusc.2015.07.086.
94 W. Hou, J. Zhou, C. Yu, S. You, X. Gao and Z. Luo, *Ind. Eng. Chem. Res.*, 2014, **53**, 9909–9914.
95 D. J. Couling, H. V. Nguyen and W. H. Green, *Chem. Eng. Sci.*, 2012, **80**, 128–133.
96 S. B. Ghorishi, C. W. Lee, W. S. Jozewicz and J. D. Kilgroe, *Environ. Eng. Sci.*, 2005, **22**, 221–231.
97 P. Guo, X. Guo and C.-g. Zheng, *Fuel*, 2011, **90**, 1840–1846.
98 K. C. Galbreath, C. J. Zygarlicke, J. E. Tibbetts, R. L. Schulz and G. E. Dunham, *Fuel Process. Technol.*, 2004, **86**, 429–448.
99 P. Guo, X. Guo and C. Zheng, *Appl. Surf. Sci.*, 2010, **256**, 6991–6996.
100 P. Liao, J. A. Keith and E. A. Carter, *J. Am. Chem. Soc.*, 2012, **134**, 13296–13309.
101 C. Loschen, J. Carrasco, K. M. Neyman and F. Illas, *Phys. Rev. B: Condens. Matter Mater. Phys.*, 2007, **75**, 035115.
102 G. Xin, P. Zhao and C. Zheng, *Proc. Combust. Inst.*, 2009, **32**, 2693–2699.
103 P. Blowers and B. G. Kim, *J. Mol. Model.*, 2011, **17**, 505–514.
104 B. Delley, *J. Chem. Phys.*, 1990, **92**, 508–517.
105 B. G. Kim, X. Li and P. Blowers, *Langmuir*, 2009, **25**, 2781–2789.
106 E. Sasmaz and J. Wilcox, *J. Phys. Chem. C*, 2008, **112**, 16484–16490.
107 J. He, G. K. Reddy, S. W. Thiel, P. G. Smirniotis and N. G. Pinto, *J. Phys. Chem. C*, 2011, **115**, 24300–24309.
108 A. Zhang, Z. Zhang, J. Chen, W. Sheng, L. Sun and J. Xiang, *Fuel Process. Technol.*, 2015, **135**, 25–33.
109 H. Li, C.-Y. Wu, Y. Li and J. Zhang, *Appl. Catal., B*, 2012, **111**, 381–388.
110 C. He, B. Shen, J. Chen and J. Cai, *Environ. Sci. Technol.*, 2014, **48**, 7891–7898.
111 H. Li, C. Y. Wu, Y. Li, L. Li, Y. Zhao and J. Zhang, *J. Hazard. Mater.*, 2012, **243**, 117–123.
112 J. He, G. K. Reddy, S. W. Thiel, P. G. Smirniotis and N. G. Pinto, *Energy Fuels*, 2013, **27**, 4832–4839.
113 H. Xu, J. Xie, Y. Ma, Z. Qu, S. Zhao, W. Chen, W. Huang and N. Yan, *Fuel*, 2015, **140**, 803–809.
114 B. Zhang, J. Liu, C. Zheng and M. Chang, *Chem. Eng. J.*, 2014, **256**, 93–100.
115 X. Sun, J.-Y. Hwang and S. Xie, *Fuel*, 2011, **90**, 1061–1068.
116 R. J. Baxter and P. Hu, *J. Chem. Phys.*, 2002, **116**, 4379–4381.
117 C. Bürgel, N. M. Reilly, G. E. Johnson, R. Mitric, M. L. Kimble, A. Castleman and V. Bonačic-Koutecký, *J. Am. Chem. Soc.*, 2008, **130**, 1694–1698.
118 S. Niksa and N. Fujiwara, *J. Air Waste Manage. Assoc.*, 2005, **55**, 1866–1875.
119 W. Lee and G.-N. Bae, *Environ. Sci. Technol.*, 2009, **43**, 1522–1527.
120 N. Spencer and R. Lambert, *Surf. Sci.*, 1981, **107**, 237–248.
121 Y. Zhao, M. D. Mann, J. H. Pavlish, B. A. Mibeck, G. E. Dunham and E. S. Olson, *Environ. Sci. Technol.*, 2006, **40**, 1603–1608.
122 A. A. Presto and E. J. Granite, *Platinum Met. Rev.*, 2008, **52**, 144–154.
123 Y. Zhuang, J. Laumb, R. Liggett, M. Holmes and J. Pavlish, *Fuel Process. Technol.*, 2007, **88**, 929–934.
124 S. Straube, T. Hahn and H. Koeser, *Appl. Catal., B*, 2008, **79**, 286–295.
125 Y. Cao, Z. Gao, J. Zhu, Q. Wang, Y. Huang, C. Chiu, B. Parker, P. Chu and W.-P. Pan, *Environ. Sci. Technol.*, 2007, **42**, 256–261.
126 S. Eswaran and H. G. Stenger, *Fuel Process. Technol.*, 2008, **89**, 1153–1159.
127 R. N. Sliger, J. C. Kramlich and N. M. Marinov, *Fuel Process. Technol.*, 2000, **65**, 423–438.

128 S. He, J. Zhou, Y. Zhu, Z. Luo, M. Ni and K. Cen, *Energy Fuels*, 2009, **23**, 253–259.
129 J. Yang, Q. Yang, J. Sun, Q. Liu, D. Zhao, W. Gao and L. Liu, *Catal. Commun.*, 2015, **59**, 78–82.
130 K. C. Galbreath and C. J. Zygarlicke, *Fuel Process. Technol.*, 2000, **65–66**, 289–310.
131 S. Wu, M. Azharuddin and E. Sasaoka, *Fuel*, 2006, **85**, 213–218.
132 S. Wu, T. Morimoto, M. A. Uddin, N. Togaki, S. Nagamine and E. Sasaoka, *Prepr. Pap. - Am. Chem. Soc., Div. Fuel Chem.*, 2004, **49**, 234–235.
133 L. Xue, T. Liu, X. Guo and C. Zheng, *Proc. Combust. Inst.*, 2015, **35**, 2867–2874.
134 C. Acuña-Caro, K. Brechtel, G. Scheffknecht and M. Braß, *Fuel*, 2009, **88**, 2489–2494.
135 W. Bergermayer, H. Schweiger and E. Wimmer, *Phys. Rev. B: Condens. Matter Mater. Phys.*, 2004, **69**, 195409.
136 T. Liu, L. Xue, X. Guo and C.-G. Zheng, *Fuel*, 2014, **115**, 179–185.
137 F. Kong, J. Qiu, H. Liu, R. Zhao and Z. Ai, *J. Environ. Sci.*, 2011, **23**, 699–704.
138 I. I. Novochinskii, C. Song, X. Ma, X. Liu, L. Shore, J. Lampert and R. J. Farrauto, *Energy Fuels*, 2004, **18**, 576–583.
139 H. Yang, R. Sothen, D. R. Cahela and B. J. Tatarchuk, *Ind. Eng. Chem. Res.*, 2008, **47**, 10064–10070.
140 S. Cheah, D. L. Carpenter and K. A. Magrini-Bair, *Energy Fuels*, 2009, **23**, 5291–5307.
141 W. F. Elseviers and H. Verelst, *Fuel*, 1999, **78**, 601–612.
142 H. Yang, Z. Xu, M. Fan, A. E. Bland and R. R. Judkins, *J. Hazard. Mater.*, 2007, **146**, 1–11.
143 H.-C. Hsi, M. J. Rood, M. Rostam-Abadi, S. Chen and R. Chang, *Environ. Sci. Technol.*, 2001, **35**, 2785–2791.
144 L. Daza, S. Mendioroz and J. Pajares, *Clays Clay Miner.*, 1991, **39**, 14–21.
145 K. Willett, R. Turner and J. Beauchamp, *Hazard. Waste Hazard. Mater.*, 1992, **9**, 275–288.
146 M. A. Uddin, T. Yamada, R. Ochiai, E. Sasaoka and S. Wu, *Energy Fuels*, 2008, **22**, 2284–2289.
147 B. Hall, O. Lindqvist and E. Ljungstroem, *Environ. Sci. Technol.*, 1990, **24**, 108–111.
148 B. Hall, P. Schager and O. Lindqvist, *Water, Air, Soil Pollut.*, 1991, **56**, 3–14.
149 N. Widmer, J. Cole, W. R. Seeker and J. Gaspar, *Combust. Sci. Technol.*, 1998, **134**, 315–326.
150 R. Meij, L. H. Vredenbregt and H. T. Winkel, *J. Air Waste Manage. Assoc.*, 2002, **52**, 912–917.
151 C. L. Senior, A. F. Sarofim, T. Zeng, J. J. Helble and R. Mamani-Paco, *Fuel Process. Technol.*, 2000, **63**, 197–213.
152 C. L. Senior, J. J. Helble and A. F. Sarofim, *Fuel Process. Technol.*, 2000, **65**, 263–288.
153 S. Wu, M. Ozaki, M. A. Uddin and E. Sasaoka, *Fuel*, 2008, **87**, 467–474.
154 M. Ozaki, M. A. Uddin, E. Sasaoka and S. Wu, *Fuel*, 2008, **87**, 3610–3615.
155 H. Li, C.-Y. Wu, Y. Li and J. Zhang, *Environ. Sci. Technol.*, 2011, **45**, 7394–7400.
156 A. Yamaguchi, H. Akiho and S. Ito, *Powder Technol.*, 2008, **180**, 222–226.
157 W. Du, L. Yin, Y. Zhuo, Q. Xu, L. Zhang and C. Chen, *Fuel Process. Technol.*, 2015, **131**, 403–408.
158 Z. Mei, Z. Shen, Q. Zhao, T. Yuan, Y. Zhang, F. Xiang and W. Wang, *Chemosphere*, 2008, **70**, 1399–1404.
159 Z. Mei, Z. Shen, Z. Mei, Y. Zhang, F. Xiang, J. Chen and W. Wang, *Appl. Catal., B*, 2008, **78**, 112–119.
160 G. Blythe, C. F. Richardson, B. W. Lani, R. G. Rhudy, M. Strohfus, L. Loritz and G. R. Energy, 2003.
161 P. Wang, S. Su, J. Xiang, F. Cao, L. Sun, S. Hu and S. Lei, *Chem. Eng. J.*, 2013, **225**, 68–75.
162 P. Wang, S. Hu, J. Xiang, S. Su, L. Sun, F. Cao, X. Xiao and A. Zhang, *Proc. Combust. Inst.*, 2015, **35**, 2847–2853.
163 W. Xu, L. Tong, H. Qi, X. Zhou, J. Wang and T. Zhu, *Ind. Eng. Chem. Res.*, 2015, **54**, 146–152.
164 X. Fan, C. Li, G. Zeng, X. Zhang, S. Tao, P. Lu, S. Li and Y. Zhao, *Fuel Process. Technol.*, 2012, **104**, 325–331.
165 X. Fan, C. Li, G. Zeng, X. Zhang, S. Tao, P. Lu, Y. Tan and D. Luo, *Energy Fuels*, 2012, **26**, 2082–2089.
166 S. Qiu, R. Ohnishi and M. Ichikawa, *J. Phys. Chem.*, 1994, **98**, 2719–2721.
167 M.-S. Liao, M.-J. Huang and J. D. Watts, *Mol. Phys.*, 2012, **110**, 3061–3076.
168 D. C. Sorescu and B. M. Rice, *J. Phys. Chem. C*, 2010, **114**, 6734–6748.
169 M. Swart, M. Solà and F. M. Bickelhaupt, *J. Comput. Chem.*, 2011, **32**, 1117–1127.
170 S. Grimme, *Wiley Interdiscip. Rev.: Comput. Mol. Sci.*, 2011, **1**, 211–228.
171 L. Goerigk and S. Grimme, *Phys. Chem. Chem. Phys.*, 2011, **13**, 6670–6688.
172 E. R. Johnson, I. D. Mackie and G. A. DiLabio, *J. Phys. Org. Chem.*, 2009, **22**, 1127–1135.
173 G. Feng, Z.-H. Lu, D. Yang, D. Kong and J. Liu, *Microporous Mesoporous Mater.*, 2014, **199**, 83–92.
174 G. Feng, Y.-Y. Lian, D. Yang, J. Liu and D. Kong, *Can. J. Chem.*, 2013, **91**, 925–934.
175 H. Fang, P. Kamakoti, J. Zang, S. Cundy, C. Paur, P. I. Ravikovitch and D. S. Sholl, *J. Phys. Chem. C*, 2012, **116**, 10692–10701.
176 J. Liu, Z.-F. Liu, G. Feng and D. Kong, *J. Phys. Chem. C*, 2014, **118**, 18496–18504.
177 G. Feng, D. Yang, D. Kong, J. Liu and Z.-H. Lu, *RSC Adv.*, 2014, **4**, 47906–47920.